

Measurement of the Pion Form Factor in the Range 1.04–1.38 GeV with the CMD-2 Detector

V. M. Aul'chenko^{a, b}, R. R. Akhmetshin^a, V. Sh. Banzarov^a, L. M. Barkov^{a, b}, N. S. Bashtovoi^a,
D. V. Bondarev^{a, b}, A. E. Bondar'^a, A. V. Bragin^a, A. A. Valishev^a, N. I. Gabyshev^a,
D. A. Gorbachev^a, A. A. Grebenyuk^a, D. N. Grigor'ev^{a, b}, S. K. Dhawan^c, D. A. Epifanov^a,
A. S. Zaitsev^{a, b}, S. G. Zverev^a, F. V. Ignatov^a, V. F. Kazanin^{a, b}, S. V. Karpov^a, I. A. Koop^{a, b},
P. P. Krokovny^{a, b}, A. S. Kuz'min^{a, b}, I. B. Logashenko^{a, d}, P. A. Lukin^a, A. P. Lysenko^a,
A. I. Mil'shtein^{a, b}, K. Yu. Mikhailov^a, I. N. Nesterenko^{a, b}, M. A. Nikulin^{a, b}, A. V. Otboev^a,
V. S. Okhupkin^a, E. A. Perevedentsev^{a, b}, A. A. Polunin^a, A. S. Popov^a, S. I. Redin^a,
B. L. Roberts^d, N. I. Root^a, A. A. Ruban^a, N. M. Ryskulov^a, A. L. Sibidanov^a, V. A. Sidorov^a,
A. N. Skrinsky^a, V. P. Smakhtin^c, I. G. Snopkov^a, E. P. Solodov^{a, b}, J. A. Thompson^{f, †},
G. V. Fedotovitch^{a, b}, B. I. Khazin^{a, b}, V. W. Hughes^{c, †}, A. G. Shamov^a, Yu. M. Shatunov^a,
B. A. Shwartz^{a, b}, S. I. Éidel'man^{a, b}, and Yu. V. Yudin^a

^a Budker Institute of Nuclear Physics, Siberian Division, Russian Academy of Sciences,
pr. Akademika Lavrent'eva 11, Novosibirsk, 630090 Russia

e-mail: ignatov@inp.nsk.su

^b Novosibirsk State University, ul. Pirogova 2, Novosibirsk, 630090 Russia

^c Yale University, New Haven, CT 06511, USA

^d Boston University, Boston, MA 02215, USA

^e Weizmann Institute of Science, 76100 Rehovot, Israel

^f University of Pittsburg, PA 15260, USA

Received November 9, 2005

The cross section for the process $e^+e^- \rightarrow \pi^+\pi^-$ is measured in the c.m. energy range 1.04–1.38 GeV by analyzing 995 000 selected collinear events including 860 000 e^+e^- events, 82 000 $\mu^+\mu^-$ events, and 33 000 $\pi^+\pi^-$ events. The systematic and statistical errors of measuring the pion form factor are equal to 1.2–4.2 and 5–13%, respectively. © 2005 Pleiades Publishing, Inc.

PACS numbers: 13.25.-k, 13.40.Gp, 13.66.-a, 29.30.-h

INTRODUCTION

Study of the cross section for the process $e^+e^- \rightarrow \pi^+\pi^-$ provides important information on the electromagnetic form factor of the pion, which describes its internal structure. Moreover, precision measurement of this cross section is necessary for calculating the anomalous magnetic moment of the muon $(g-2)_\mu$ [1] and its comparison with precision measurements, one of which was carried out recently at BNL [2]. Such comparison is an important test for the Standard Model.

EXPERIMENT

Measurements were conducted at the VEPP-2M collider [3] with the CMD-2 universal detector (cryogenic magnetic detector), which combines the properties of a magnetic spectrometer and good calorimetry [4, 5]. The coordinates, emission angles, and momenta

of charged particles are measured by the coordinate system of the detector, which consists of the drift and Z chambers located inside a thin ($0.38X_0$) superconducting solenoid with a magnetic field of 1 T. Cylindrical and endcap electromagnetic calorimeters based on CsI and BGO scintillation crystals ensure measurement of energy and photon emission angles and make it possible to separate electrons and hadrons. A range system is used to identify muons.

This work continues a cycle of precision measurements of hadron cross sections with the CMD-2 detector. The results of measurement of the pion form factor in the energy range 0.61–0.96 GeV were published in [6]. In this work, we present the results of measurement of the form factor in the energy range 1.04–1.38 GeV. A more detailed description of the data analysis was given in [7].

An integrated luminosity of 6 pb^{-1} was collected in the experiment. For analysis, we selected 33 000 $\pi^+\pi^-$ events accumulated in 35 beam energy points from 520

[†] Deceased.

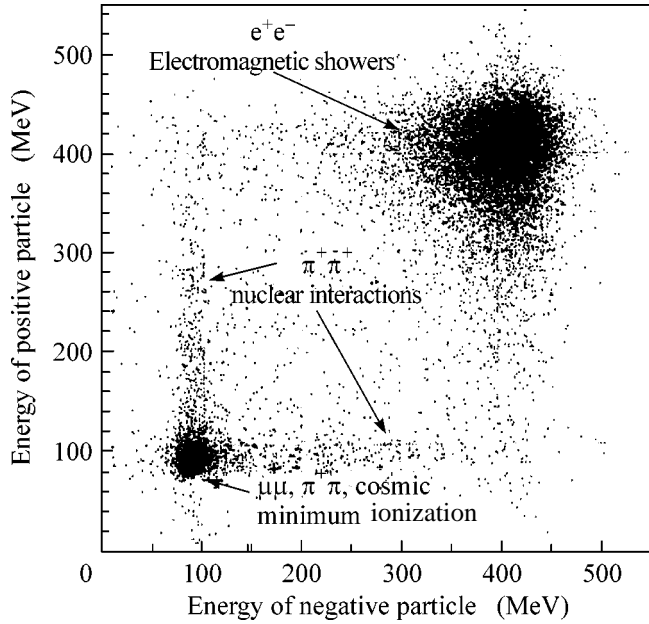


Fig. 1. Distribution of collinear particles over the energy deposition in the calorimeter.

to 690 MeV with a step of 5 MeV. The beam energy was controlled with an accuracy of no worse than $\delta E/E \sim 10^{-3}$ using the magnetic field value in the VEPP-2M storage ring.

SELECTION OF COLLINEAR EVENTS

To separate the events $e^+e^- \rightarrow e^+e^-$, $e^+e^- \rightarrow \mu^+\mu^-$, and $e^+e^- \rightarrow \pi^+\pi^-$, the following conditions were used.

- One vertex with two tracks of particles with opposite charges was found in the drift chamber.

- The event vertex was located near the beam interaction point; i.e., $\rho_{\text{vtx}} = \min(\rho_{\text{tr}}^+, \rho_{\text{tr}}^-) < 0.15$ cm, where ρ_{tr}^\pm is the minimum distance between the particle track and beam axis, and $|Z_{\text{vtx}}| < 10$ cm, where Z_{vtx} is the position of the vertex along the beam axis.

- Track collinearity conditions:

$|\Delta\phi| = |\pi - |\phi^+ - \phi^-|| < 0.15$, where ϕ^\pm is the azimuth track angle;

$|\Delta\theta| = |\pi - (\theta^+ + \theta^-)| < 0.25$, where θ^\pm is the polar track angle.

- Constraint on the solid angle of the event detection:

$\theta_{\text{min}} < (\pi + \theta^- - \theta^+)/2 < \pi - \theta_{\text{min}}$, where $\theta_{\text{min}} = 1.1$.

- The mean momentum was bounded from above to reduce the cosmic particle background and from below to suppress $e^+e^- \rightarrow K^+K^-$ events:

$$E_{\text{beam}} + 150 \text{ MeV}/c > (p^+ + p^-)/2 \\ > \max(\sqrt{E_{\text{beam}}^2 - 494^2} \times 1.15 \text{ MeV}/c, 300 \text{ MeV}/c),$$

where p^+ and p^- are the momenta of the positive and negative particles, respectively.

The main sources of the background for the process $e^+e^- \rightarrow \pi^+\pi^-$ are the $e^+e^- \rightarrow \pi^+\pi^-\pi^0\pi^0$, $e^+e^- \rightarrow \pi^+\pi^-\pi^0$, and $e^+e^- \rightarrow K^+K^-$ reactions and cosmic particles. The physical background contribution to the pion form factor was calculated using experimental cross sections [8, 9] by taking into account the detection efficiency determined from the total simulation. The total contribution of these processes does not exceed 0.8% and is taken into account as a correction to the pion form factor according to Eq. (2). The number of cosmic particle background events was determined from the distribution of the event vertices over the distance from the beam interaction point.

EVENT SEPARATION

To determine the number of events of each process, we used two-dimensional distributions over the energy deposition in the CsI calorimeter (Fig. 1). The number of events ($N_\pi, N_\mu + N_e$) was determined by minimizing the maximum likelihood function

$$\mathcal{L} = - \sum_{\text{events}} \ln \left(\sum_i N_i f_i(E^+, E^-) \right) + \sum_i N_i,$$

where f_i is the probability density function for events of a given type ($\pi, \mu, e, \text{cosmic}$). Electrons and positrons initiate an electromagnetic shower in a calorimeter and thereby noticeably differ from other charged particles in their energy deposition. The energy depositions of muons, cosmic particles, and pions with only ionization losses are almost identical. For this reason, to determine the number of muons, we used additional information on the ratio of the cross section for muon production to the cross section for $e^+e^- \rightarrow e^+e^-$ as obtained from the QED calculation with the inclusion of the resolutions and detection efficiencies in the detector.

DETERMINATION OF THE PION FORM FACTOR

The cross section for the $e^+e^- \rightarrow \pi^+\pi^-$ process integrated over the detection solid angle is given by the expression

$$\sigma_{\pi^+\pi^-} = \sigma_{\pi^+\pi^-}^0 |F_\pi|^2 \\ = \frac{\pi\alpha^2}{3s} \left(1 - \frac{4m_\pi^2}{s}\right)^{3/2} \frac{3 \cos\theta_{\text{min}} - \cos^3\theta_{\text{min}}}{2} |F_\pi|^2, \quad (1)$$

where $\sigma_{\pi^+\pi^-}^0$ is the cross section calculated under the assumption of the absence of the internal structure of the pion. The contribution of vacuum polarization to the photon propagator is also included in the form factor.

At each energy point, the form factor is calculated as

$$|F_\pi|^2 = \frac{N_{\pi^+\pi^-}}{N_{e^+e^-} + N_{\mu^+\mu^-}} \times \frac{\sigma_{e^+e^-}^0(1 + \delta_{e^+e^-})\varepsilon_{e^+e^-} + \sigma_{\mu^+\mu^-}^0(1 + \delta_{\mu^+\mu^-})\varepsilon_{\mu^+\mu^-}}{\sigma_{\pi^+\pi^-}^0(1 + \delta_{\pi^+\pi^-})\varepsilon_{\pi^+\pi^-}(1 - \Delta_{\pi\text{loss}}) - \Delta_{3\pi, 4\pi, K^+K^-}} \quad (2)$$

Here, $N_{\pi^+\pi^-}/(N_{e^+e^-} + N_{\mu^+\mu^-})$ is the ratio of the number of detected pions to the number of muons and electrons as obtained in the minimization procedure, σ_{ii}^0 is the Born cross section in the lowest order of perturbation theory, δ_{ii} is the radiative correction, ε_{ii} is the detection efficiency, $\Delta_{3\pi, 4\pi, K^+K^-}$ is the correction for background processes, and Δ_{loss} is the correction for the pion loss on the vacuum chamber wall and drift chamber material due to nuclear interactions. The Δ_{loss} correction was determined from simulation by comparing the number of selected pions with the inclusion and exclusion of nuclear interactions. The correction value was equal to 0.8–1.2%.

Collinear events were selected using only information from the drift chamber. For this reason, by selecting desired (test) events from the CsI calorimeter and checking whether the reconstructed tracks are in the drift chamber, one can determine the event reconstruction efficiency. The reconstruction efficiency was 97–98%. According to Eq. (2), only the difference between the detection efficiencies for different processes, which was $0.16 \pm 0.09\%$ between electrons and muons, is important for the determination of the pion form factor.

The radiative corrections for the processes $e^+e^- \rightarrow e^+e^-$, $e^+e^- \rightarrow \mu^+\mu^-$, and $e^+e^- \rightarrow \pi^+\pi^-$ are calculated using a procedure that was developed in [10] and was based on the formulas from [11, 12]. The probability of the emission of many photons along the initial and final particles, the emission of one photon at a large angle, and the vacuum polarization contribution to the photon propagator are taken into account in these formulas. Since the vacuum polarization is usually included in the definition of the form factor, its contribution was not included in the radiative correction for the process $e^+e^- \rightarrow \pi^+\pi^-$. According to [10], the accuracy of the calculation of the radiative corrections is estimated as 0.2% for all the processes. The number of selected collinear events depends on the angular and momentum resolutions of the drift chamber. In order to include them in the calculation for radiative corrections, the emission angles and momenta of particles were addi-

Table 1. Experimental pion form factor $|F_\pi|^2$. Only the statistical error is given

E , MeV	$ F_\pi ^2$	E , MeV	$ F_\pi ^2$
490.0	3.596 ± 0.163	605.7	1.069 ± 0.082
520.0	2.598 ± 0.134	610.0	0.989 ± 0.075
525.0	2.262 ± 0.112	615.0	1.069 ± 0.088
530.0	2.185 ± 0.135	620.0	0.988 ± 0.081
535.0	2.295 ± 0.130	625.0	0.794 ± 0.064
540.0	1.884 ± 0.119	630.0	0.696 ± 0.063
545.0	2.120 ± 0.110	635.0	0.719 ± 0.057
550.0	1.704 ± 0.120	640.0	0.693 ± 0.052
555.0	1.641 ± 0.106	645.0	0.571 ± 0.042
560.0	1.449 ± 0.146	650.0	0.640 ± 0.046
565.0	1.683 ± 0.103	655.0	0.570 ± 0.050
570.0	1.531 ± 0.088	660.0	0.483 ± 0.054
575.0	1.374 ± 0.150	665.0	0.460 ± 0.040
580.0	1.386 ± 0.087	670.0	0.524 ± 0.062
585.0	1.197 ± 0.115	675.0	0.347 ± 0.049
590.0	1.200 ± 0.088	680.0	0.357 ± 0.040
595.0	1.014 ± 0.093	685.0	0.424 ± 0.078
600.0	0.983 ± 0.079	690.0	0.338 ± 0.032

tionally simulated according to the experimental resolution and then the selection criteria were imposed. For the $e^+e^- \rightarrow e^+e^-$ process, the bremsstrahlung energy losses of electrons and positrons on the vacuum chamber wall and first 10 cm of the drift chamber were taken into account.

Table 1 presents the form factor at each energy point.

SYSTEMATIC ERROR

The main contributions to the systematic error are listed in Table 2. The systematic error increases with energy, because the error in the number of muons makes a direct contribution to the error in the number of pions, and the ratio of the number of muons to the number of pions increases from 1 to 7 when the c.m. energy increases from 1 to 1.38 GeV. The total systematic error is equal to 1.2–4.2% and does not exceed one-third of the statistical error at each experimental point.

One of the tests of the separation procedure was performed using the simulation of e^+e^- , $\mu^+\mu^-$, and $\pi^+\pi^-$ events. The simulation data were analyzed with the inclusion of the following corrections: pion loss due to the nuclear interaction, the energy losses of electrons on the vacuum-chamber wall, and the resolution of the drift chamber when calculating radiative corrections. The calculated difference between the detection efficiencies for e^+e^- and $\mu^+\mu^-$, $\pi^+\pi^-$ in the simulation was

Table 2. Various contributions to the systematic error in $|F_\pi|^2$. The given range corresponds to the scanned energy range

Error source	Error $\sqrt{s} = 1.04\text{--}1.38$ GeV
Detection solid angle	0.2–0.5%
Detection efficiency	0.5–2%
Pion loss	0.2%
Bremsstrahlung e^+e^-	0.05–1.7%
Radiative corrections	0.5–2%
Background events	0.6–1.6%
Energy calibration	0.7–1.1%
Particle separation procedure	0.2–1.5%
Statistical error at the point	1.2–4.2%
	5–13%

equal to $\varepsilon_{\text{MIP}} - \varepsilon_{e^+e^-} = 0.189 \pm 0.004\%$ in good agreement with the measured value. The difference between the form factor obtained and the form factor used in the simulation varies from 0.2 to 1.5% in dependence on the energy. The difference at the highest energy was equal to 1.5% and consisted of 1% for the separation procedure and 0.5% characterizing the systematic error in the inclusion of the above corrections.

DISCUSSION

Figure 2 shows the results, which are in good agreement with the data obtained in the previous experiments with the detectors OLYA [13], DM1 [14], DM2 [15], BCF [16], and ACO [17]. The form factor in this energy range was measured in detail only in the experiment with the OLYA detector with a systematic error of 10–15%. The experimental energy dependence of the form

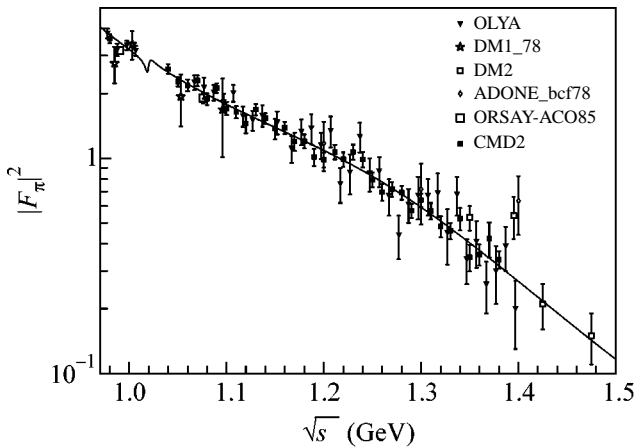


Fig. 2. Experimental data obtained for the pion form factor $|F_\pi|^2$ in this work in comparison with other experiments.

factor is well reproduced in the framework of the vector-meson dominance model by the sum of the amplitudes of the $\rho(770)$, $\rho(1450)$, $\rho(1700)$, ω , and ϕ mesons [6]:

$$|F_\pi(s)|^2 = \left| \left(\text{BW}_{\rho(770)}^{\text{GS}}(s) \right) \times \left(1 + \delta_\omega \frac{s}{m_\omega^2} \text{BW}_\omega(s) + \delta_\phi \frac{s}{m_\phi^2} \text{BW}_\phi(s) \right) + \beta \text{BW}_{\rho(1450)}^{\text{GS}}(s) + \gamma \text{BW}_{\rho(1700)}^{\text{GS}}(s) \right|^2 / (1 + \beta + \gamma)^2. \quad (3)$$

Here, $\text{BW}_\rho^{\text{GS}}(s)$ is the ρ meson parametrization in the Gounaris–Sakurai model [18]; $\text{BW}_\omega(s)$ and $\text{BW}_\phi(s)$ are the parametrization of the ω and ϕ resonances, respectively, which were represented by the relativistic Breit–Wigner form due to small width; δ_ω , δ_ϕ , β , and γ are the model parameters describing the relative contributions of the ρ – ω and ρ – ϕ interferences and $\rho(1450)$ and $\rho(1700)$ states, respectively. In order to determine the model parameters, it is necessary to use all the available data on the form factor in the energy range $\sqrt{s} = 0.36\text{--}3.7$ GeV, which will be done in a future work with analysis of all the information accumulated on the CMD-2 detector in the energy range from 0.37 to 1.38 GeV.

CONCLUSIONS

In this work, the cross section for the process $e^+e^- \rightarrow \pi^+\pi^-$ was measured in the c.m. energy range 1.04–1.38 GeV with the best accuracy in the world. The systematic and statistical errors of the measurement are equal to 1.2–4.2 and 5–13%, respectively. The measured cross section agrees well with the results of the previous experiments.

This work was supported by the Russian Foundation for Basic Research (project nos. 03-02-16477, 03-02-16280, 03-02-16843, 04-02-16217, 04-02-16223, and 04-02-16434).

REFERENCES

1. M. Davier and W. J. Marciano, *Annu. Rev. Nucl. Part. Sci.* **54**, 115 (2004).
2. G. W. Bennett *et al.*, *Phys. Rev. Lett.* **92**, 161802 (2004).
3. V. V. Anashin, I. B. Vasserman, V. G. Veshcherevich, *et al.*, Preprint No. 84-114, IYaF (Inst. of Nuclear Physics, Siberian Division, USSR Academy of Sciences, Novosibirsk, 1984).
4. G. A. Aksenov, V. M. Aul'chenko, L. M. Barkov, *et al.*, Preprint No. 85-118, IYaF (Inst. of Nuclear Physics, Siberian Division, USSR Academy of Sciences, Novosibirsk, 1985).
5. E. V. Anashkin, V. M. Aulchenko, S. E. Baru, *et al.*, *ICFA Instrum. Bull.* **5**, 18 (1988).

6. R. R. Akhmetshin *et al.*, Phys. Lett. B **527**, 161 (2002); Phys. Lett. B **578**, 285 (2004).
7. V. M. Aul'chenko, R. R. Akhmetshin, V. Sh. Banzarov, *et al.*, Preprint No. 2005-29, IYaF (Inst. of Nuclear Physics, Siberian Division, Russian Academy of Sciences, Novosibirsk, 2005).
8. R. R. Akhmetshin *et al.*, Phys. Lett. B **489**, 125 (2000).
9. R. R. Akhmetshin *et al.*, Phys. Lett. B **466**, 392 (1999).
10. A. B. Arbuzov, G. V. Fedotovitch, F. V. Ignatov, *et al.*, Preprint INP 04-70 (Inst. of Nuclear Physics, Siberian Division, Russian Academy of Sciences, Novosibirsk, 2004).
11. A. B. Arbuzov, E. A. Kuraev, V. A. Astakhov, *et al.*, J. High Energy Phys. **10**, 006 (1997).
12. A. B. Arbuzov, E. A. Kuraev, G. V. Fedotovitch, *et al.*, J. High Energy Phys. **10**, 001 (1997).
13. L. M. Barkov *et al.*, Nucl. Phys. B **256**, 365 (1985).
14. A. Quenzer *et al.*, Phys. Lett. B **76**, 512 (1978).
15. D. Bisello *et al.*, Phys. Lett. B **220**, 321 (1989).
16. D. Bollini *et al.*, Lett. Nuovo Cimento **14**, 418 (1975).
17. G. Cosme *et al.*, Preprint LAL-1287 (Orsay, 1976).
18. G. J. Gounaris and J. J. Sakurai, Phys. Rev. Lett. **21**, 244 (1968).

Translated by R. Tyapayev

Quantum Instability in Cavity QED

S. V. Prants and M. Yu. Uleysky

*Pacific Oceanological Institute, Far East Division, Russian Academy of Sciences,
ul. Baltiiskaya 43, Vladivostok, 690041 Russia*

e-mail: prants@poi.dvo.ru

Received October 26, 2005

The stability and instability of quantum evolution are analyzed in the interaction of a two-level atom with a quantized-field mode in an ideal cavity with allowance for photon recoil, which is the basic model of cavity QED. It is shown that the Jaynes–Cummings quantum dynamics can be unstable in the regime of the random walk of the atom in the quantized field of a standing wave in the absence of any interaction with the environment. This instability is manifested in large fluctuations of the quantum entropy, which correlate with a classical-chaos measure, the maximum Lyapunov exponent, and in the exponential sensitivity of the fidelity of the quantum states of the strongly coupled atom–field system to small variations of resonance detuning. Numerical experiments reveal the sensitivity of the atomic population inversion to the initial conditions and to correlation between the quantum and classical degrees of freedom of the atom. © 2005 Pleiades Publishing, Inc.

PACS numbers: 05.45.Mt, 05.45.Xt, 42.50.Vk

The problem of the stability of quantum evolution is important as a fundamental problem of modern quantum mechanics. It is difficult to overestimate its importance for actively developing areas such as quantum information and quantum computations. This problem is a foundation stone of quantum–classical correspondence, which is brightly manifested in the following contradiction: conventional quantum mechanics does not involve the instability concept and its extreme manifestation—dynamical chaos unconditionally existing in nature. The point is not about the probability nature of quantum mechanics. Classical mechanics can also be formulated in probability terms by means of the Liouville equation. In contrast to continuous classical phase space, the phase space of an isolated quantum system is discrete. Therefore, mixing in volumes less than \hbar^N , where N is the number of degrees of freedom [1], which is characteristic of chaos, cannot be developed in it. The solution to this problem is suggested by a simple argument—real quantum systems are not isolated due to their inevitable interaction with the environment. The environment rapidly destroys quantum coherence (see references on decoherence, e.g., [2, 3]) and weak continuous measurements in the environment roughen quantum evolution and can result in quantum–classical correspondence including chaos (see references on conditioned evolution and stochastic quantum equations, e.g., [4, 5]).

In this work, we show that the entanglement of the quantum states of the atom and field is dynamically consistent with the motion of the center of mass of the atom in the field of the standing light wave in the cavity. The regular motion of the center of mass corresponds to the regular evolution of reduced quantum entropy and

to the fidelity of quantum states, and quantum evolution becomes unstable when the motion of the center of mass is chaotic. Novelty is in the appearance of quantum instability characterized by the classical Lyapunov exponent and in the manifestations of dynamical chaos in a quantum–classical system without involving complex models of interaction with the external world, whose role is played by the translational degree of freedom of the atom. Using numerical experiments, we demonstrate the diverse manifestations of quantum–classical correspondence including dynamical chaos, which can be observed in real experiments with atoms and photons in high- Q cavities.

A measure of classical instability is the maximum Lyapunov exponent λ , which characterizes the asymptotic velocity of the exponential divergence of two initially close trajectories. Ideally isolated quantum systems are unitary and their evolution cannot be classically unstable even if their classical limits are chaotic [1]. As a measure of quantum instability, Peres [6] proposed the fidelity

$$f(t) = |\langle \Psi_1(t) | \Psi_2(t) \rangle|^2, \quad (1)$$

which is the overlap integral of two wave functions Ψ_1 and Ψ_2 that coincide with each other at the initial time $t = 0$ but evolve with slightly different Hamiltonians.

The standard Hamiltonian of cavity QED has the form

$$\hat{H} = \frac{\hat{p}^2}{2m_a} + \frac{1}{2}\hbar\omega_a\hat{\sigma}_z + \hbar\omega_f\hat{a}^\dagger\hat{a} - \hbar\Omega_0(\hat{a}^\dagger\hat{\sigma}_- + \hat{a}\hat{\sigma}_+)\cos k_f\hat{x}, \quad (2)$$

where $\hat{\sigma}_{\pm,z}$ are the Pauli operators, and describes the interaction between a two-level atom, which has lower $|1\rangle$ and upper $|2\rangle$ energy states with the energy difference $\hbar\omega_a$ between them, and a mode of the quantized electromagnetic field with the creation \hat{a}^\dagger and annihilation \hat{a} operators, which forms a one-dimensional standing wave with the frequency ω_f and wavenumber k_f in an ideal cavity. The position of the atom with mass m_a on the cavity axis x is described by the operator \hat{x} and its momentum, by the operator \hat{p} . The interaction results in the quantum entanglement of the internal electronic degrees of freedom of the atom and the degrees of freedom of the field. This entanglement is described by the vector of state of the atom–field system at the time t

$$|\Psi(t)\rangle = \sum_{n=0}^{\infty} a_n(t)|2, n\rangle + b_n(t)|1, n\rangle, \quad (3)$$

which is expanded in the basis of the Fock field states $|n\rangle$, where $n = 0, 1, \dots$. Here, $a_n(t) \equiv \alpha_n(t) + i\beta_n(t)$ and $b_n(t) \equiv \rho_n(t) + i\eta_n(t)$ are the complex probability amplitudes for the field in the state $|n\rangle$ and the atom in the upper $|2\rangle$ and lower $|1\rangle$ energy states, respectively. Emission and absorption of photons change not only the internal state of the atom but also its translational state. If atoms are not too cold and their mean momentum is much higher than the photon momentum $\hbar k_f$, the translational degree of freedom can be described classically. Such a simplification is additionally motivated because the position of the atom in the cavity in the current experiments [7] is monitored by weak continuous measurement of scattered photons and, as a result, the atomic trajectory becomes classical.

The complete dynamics (in the framework of the above assumptions) are described by the Hamilton–Schrödinger equations [8, 9] written in the reference frame rotating with the frequency $\omega_f(n + 1/2)$ in the normalized form

$$\begin{aligned} \dot{x} &= \omega_r p, \\ \dot{p} &= -2 \sin x \sum_{n=0}^{\infty} \sqrt{n+1} (\alpha_n \rho_{n+1} + \beta_n \eta_{n+1}), \\ \dot{\alpha}_n &= -\frac{\delta}{2} \beta_n - \sqrt{n+1} \eta_{n+1} \cos x, \\ \dot{\beta}_n &= \frac{\delta}{2} \alpha_n + \sqrt{n+1} \rho_{n+1} \cos x, \\ \dot{\rho}_{n+1} &= \frac{\delta}{2} \eta_{n+1} - \sqrt{n+1} \beta_n \cos x, \\ \dot{\eta}_{n+1} &= -\frac{\delta}{2} \rho_{n+1} + \sqrt{n+1} \alpha_n \cos x, \end{aligned} \quad (4)$$

where $x = k_f \langle \hat{x} \rangle$ and $p = \langle \hat{p} \rangle / \hbar k_f$ are the coordinate and average momentum of the atomic center of mass, respectively. The overdot stands for differentiation with respect to the dimensionless time $\tau = \Omega_0 t$, where Ω_0 is the amplitude of the atom–field coupling constant.

Equations (4) compose an infinite-dimensional nonlinear dynamical system with two control parameters, normalized resonance detuning $\delta = (\omega_f - \omega_a) / \Omega_0$ and normalized atomic recoil frequency $\omega_r = \hbar k_f^2 / m_a \Omega_0 \ll 1$. Although the number of the integral of motion

$$R_n = \alpha_n^2 + \beta_n^2 + \rho_{n+1}^2 + \eta_{n+1}^2 = \text{const}, \quad \sum_{n=0}^{\infty} R_n \leq 1, \quad (5)$$

is infinite and the total energy

$$\begin{aligned} W &= \frac{\omega_r p^2}{2} - \frac{\delta}{2} \sum_{n=0}^{\infty} (\alpha_n^2 + \beta_n^2 - \rho_{n+1}^2 - \eta_{n+1}^2) \\ &\quad - 2 \cos x \sum_{n=0}^{\infty} \sqrt{n+1} (\alpha_n \rho_{n+1} + \beta_n \eta_{n+1}) \end{aligned} \quad (6)$$

is conserved, this system is generally nonintegrable.

The type of the motion of the atomic center of mass depends strongly on the detuning δ . At exact resonance for atoms prepared at $\tau = 0$ in one of the energy states, the optical potential vanishes and the atoms move with a constant velocity $\dot{x} = \omega_r p_0$. Quantum evolution is strictly periodic with the period $\pi / \omega_r p_0$. It is easy to explicitly find the exact solutions for the purity of the state, the von Neumann quantum entropy, the fidelity, and other quantum characteristics. In particular, the atomic population inversion at $\delta = 0$ has the form

$$\begin{aligned} z(\tau) &= \sum_{n=0}^{\infty} z_n = \sum_{n=0}^{\infty} z_n(0) \cos\left(\frac{2\sqrt{n+1}}{\omega_r p_0} \sin \omega_r p_0 \tau\right), \\ z_n &= \alpha_n^2 + \beta_n^2 - \rho_{n+1}^2 - \eta_{n+1}^2. \end{aligned} \quad (7)$$

If the detuning is large enough; i.e., $|\delta| \gg 0$, the optical potential wells are shallow and the atoms move with the average velocity $\approx \omega_r p_0$, which is only slightly modulated by the standing wave. The population inversion also oscillates with a small amplitude except for in the Doppler–Rabi resonance case [10] under the condition $|\delta| = \omega_r |p_0|$. If the kinetic energy $\omega_r p^2 / 2$ of the atom is not enough to overcome the optical potential barrier, the atomic center of mass undergoes nonlinear oscillations in one of the potential wells.

According to the form of the Hamilton–Schrödinger equations (4), the translational motion of the atom is described by the nonlinear-oscillator equation with modulated frequency. The analysis performed in [11] for an equation of such type shows that, owing to inter-

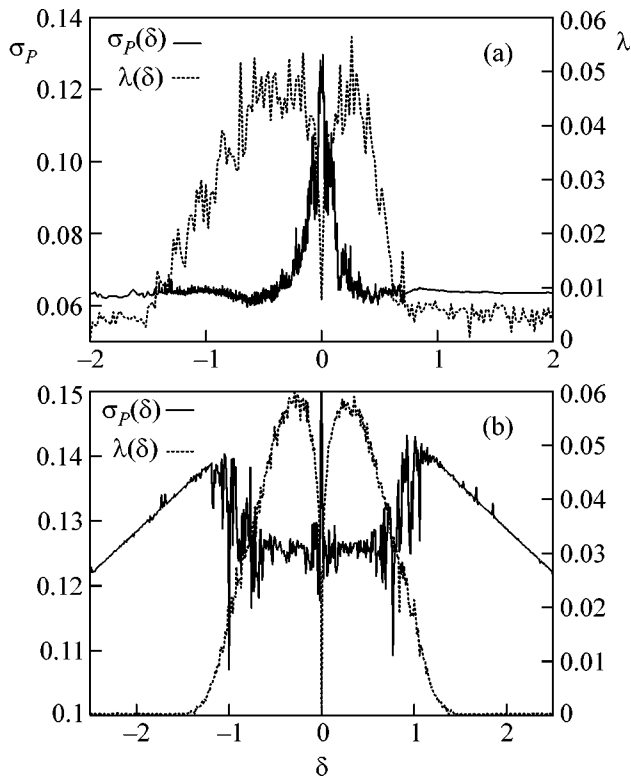


Fig. 1. Quantum-classical correlation of the dependences of the standard deviation of the quantum-state purity σ_P and maximum Lyapunov exponent λ on the detuning δ of the atomic-field resonance for (a) coherent and (b) Fock initial states of the field.

actions between nonlinear resonances, a stochastic layer whose width depends on δ appears in the corresponding phase space. When the detunings are moderate; i.e., $|\delta| \lesssim 1$, and the initial momentum is appropriate, the atom randomly walks over the cavity and such a motion is well characterized by positive values of the maximum Lyapunov exponent. The dotted line in Fig. 1 shows the dependence $\lambda(\delta)$ calculated for Eqs. (4) with the initial conditions $x_0 = 0$ and $p_0 = 25$ (a) for the atom prepared in the state $|2\rangle$ and the field in the coherent state with the average number of photons $\bar{n} = 10$ and (b) for the atom prepared in the state $(|1\rangle + |2\rangle)/\sqrt{2}$ and the field in the Fock state with $n = 10$. The normalized recoil frequency is taken to be $\omega_r = 0.001$, which is a reasonable value for atoms in a high- Q optical microcavity under strong coupling conditions [7].

Let us now demonstrate how the classical motion of the atomic center of mass correlates with the Jaynes-Cummings quantum dynamics [3]. As a measure of the entanglement of the atomic and field states, we take the purity of the state $P(\tau) = \text{Tr} \rho_a^2(\tau)$, where $\rho_a(\tau)$ is the reduced atomic density matrix with averaging over the field states. This quantity is maximal if the atom is in

one of its energy states, $P_{\max} = \text{Tr} \rho_a^2 = \text{Tr} \rho_a = 1$, and is minimal, $P_{\min} = 1/2$, if $\rho_a = I/2$, where I is the identity matrix. The purity is expressed in terms of the probability amplitudes as

$$P = \left(\sum_{n=0}^{\infty} (\alpha_n^2 + \beta_n^2) \right)^2 + \left(\sum_{n=0}^{\infty} (\rho_n^2 + \eta_n^2) \right)^2 + 2 \left(\sum_{n=0}^{\infty} (\alpha_n \rho_n + \beta_n \eta_n) \right)^2 - 2 \left(\sum_{n=0}^{\infty} (\alpha_n \eta_n + \beta_n \rho_n) \right)^2. \quad (8)$$

Varying the resonance detuning δ , we can cause the atomic center of mass to move in one of the above regimes: ballistic flight ($|\delta| = 0$ and $|\delta| \gg 0$), nonlinear oscillations in a potential well ($|\delta| \ll 1$ and sufficiently low initial momentum), and random walk ($|\delta| \lesssim 1$). According to the form of the Hamilton-Schrödinger equations, P must be a complexly oscillating function of time, because these equations include an infinite number of incommensurate frequencies. To reveal the differences in the behaviors of P in different motion regimes of the center of mass, we calculate the standard

deviation $\sigma_P = \sqrt{\langle P^2 \rangle - \langle P \rangle^2}$ of the atomic-state purity in a wide time interval $\tau = 2000$ for various initial states of the atom and field. The detuning dependence of this quantity is shown by the solid line in Fig. 1. Irregular oscillations in σ_P were found to be observed for both coherent and Fock fields under the same initial conditions and in the same detuning interval $|\delta| \lesssim 1$, where $\lambda > 0$. As was expected, the calculated variations in the von Neumann quantum entropy $S = -\text{Tr}(\rho_a \ln \rho_a)$, which are not shown in the figure, also correlate with the maximum Lyapunov exponent. For the simplest initial state with the atom prepared in the state $|2\rangle$ and the field in the Fock state $|n\rangle$, entanglement occurs between two quantum two-level systems (the atom with the states $|1\rangle$ and $|2\rangle$ and the field with the states $|n\rangle$ and $|n+1\rangle$) and is described by only six equations (4) with a fixed n value. The purity is determined by the Rabi oscillations of the atomic population inversion z_n by the formula

$$P_n = \frac{1}{2} (1 + z_n^2). \quad \text{At } |\delta| = 0, \text{ these are periodic oscillations; at } |\delta| \gg 0, \text{ regular amplitude modulated oscillations; and, at } |\delta| \lesssim 1 \text{ (and appropriate initial momentum), the Rabi oscillations become chaotic with almost unpredictable changes in } z_n \text{ when the atom intersects nodes of the standing wave in the process of its random walk. Chaotic oscillations of the population inversion } z_n \text{ and atomic-state purity } P_n \text{ arise only if } \lambda > 0.$$

The atomic coordinate x and population inversion z are experimentally measurable quantities. Similar to the case of a classical standing wave [12], the chaotic motion of the atom in the quantized field has fractal properties. Let atoms be placed one-by-one at the cor-

dinate origin ($x = 0$) with various initial momenta p_0 along the x axis and with the same initial values of the other variables and the same parameters. We calculate both the time $T(p_0)$ in which the atom with a given p_0 value approaches one of the standing wave nodes closest to the coordinate origin ($x = -\pi/2$ and $3\pi/2$) and the number m of changes in the direction of the atom motion. The scattering function $T(p_0)$ has the self-similar structure with alternating smooth sections and sections with poor resolution, a further increase in which reproduces the same structure of alternating sections. Figure 2a shows the scheme of generating a Cantorlike set of initial momenta p_0 at which the scattering function has singularities. We emphasize that the interaction between the classical and quantum degrees of freedom of the single atom and one field mode is so complicated that, within one period of the standing wave, there exist an infinite number of atomic trajectories with various p_0 values for which $T \rightarrow \infty$. The results of calculation of $T(p_0)$ for many periods of the standing wave are very similar; however, they require much longer computation time. We find that the infinitely large countable set of separatrix-like trajectories corresponding to the section ends in Fig. 2a exists along with an uncountable set of trajectories with $m = \infty$. Manifestations of the random walk of atoms can be observed in experiments on the one-dimensional scattering of atoms on the standing light wave. Figure 2b shows the strong dependence of the atomic coordinate at a given time on its initial momentum p_0 . The smooth section of this function for $p_0 \lesssim 20$ is attributed to the regular oscillations of the atomic center of mass in the first well, because the corresponding kinetic energies are insufficient to overcome the potential barrier. As p_0 exceeds a certain critical value, it is almost impossible to predict even the sign of the atomic coordinate. The so-called predictability horizon can be estimated as $\tau_p \approx \lambda^{-1} \ln(\Delta x / \Delta x_0)$, where Δx is the confidence interval and Δx_0 is the uncertainty of the initial atomic position.

A practically important manifestation of quantum instability in the chaotic walk regime of the atom is the strong dependence of the atomic population inversion z_{out} at a given time on its initial value z_{in} under the same other conditions. Figure 2c demonstrates the smoothness of this function in the initial-value interval $|z_{\text{in}}| \lesssim 0.8$, where the motion of the atomic center of mass is regular (for the coherent-field phase chosen for calculation), and its strong fluctuations in the interval $|z_{\text{in}}| > 0.8$, when atoms chaotically walk over the cavity with the positive Lyapunov exponent.

As a quantitative characteristic of the instability of the quantum evolution in cavity QED, we can use the fidelity $f(\tau)$, which is the overlap integral (1) of two states $|\Psi_1(\tau)\rangle$ and $|\Psi_2(\tau)\rangle$ that are identical at $\tau = 0$ but

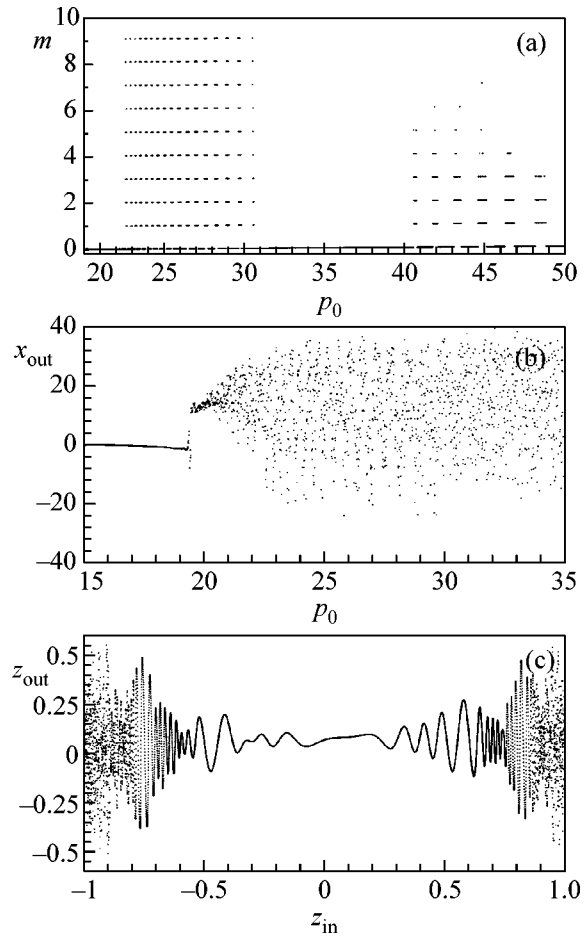


Fig. 2. (a) Fractal set of the initial momenta p_0 of atoms leaving the one-period standing wave after m changes in the motion directions. (b) The output atomic coordinate x_{out} vs. the initial momentum p_0 . (c) The output atomic population inversion z_{out} vs. its initial value z_{in} .

evolve under two Hamiltonians (2) with slightly different detunings $\Delta\delta = \delta - \delta'$:

$$f(\tau) = \left(\sum_{n=0}^{\infty} (\alpha_n \alpha'_n + \beta_n \beta'_n + \rho_n \rho'_n + \eta_n \eta'_n) \right)^2 + \left(\sum_{n=0}^{\infty} (\alpha_n \beta'_n - \beta_n \alpha'_n + \rho_n \eta'_n - \eta_n \rho'_n) \right)^2. \quad (9)$$

Here, the unprimed and primed quantities correspond to the Hamiltonians with the detunings δ and δ' , respectively. We found pronounced correlation between this characteristic of quantum evolution and the classical characteristic of the motion. If the motion of the atomic center of mass is regular and characterized by the zero Lyapunov exponent, the quantum dynamics of the atom-field system is stable and characterized by the small values of $1 - f$. If the motion of the atomic center of mass is chaotic with $\lambda > 0$, the fidelity decreases

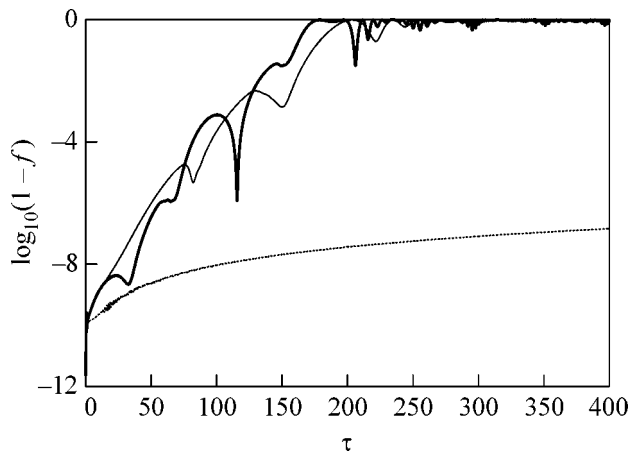


Fig. 3. Evolution of the measure of fidelity $1 - f(\tau)$ of the quantum states of the atom–field system (in the logarithmic scale) for the (thick and thin solid lines) chaotic and (dotted line) regular motion of the atomic center of mass.

exponentially with time with the exponent λ . The dotted line in Fig. 3 exemplifies stable quantum evolution [the atom is prepared in the superposition state with $z(0) = 0$, its translational motion is regular, and $\lambda = 0$]. The situation is absolutely different when the atom is prepared in one of its energy states, $z(0) = \pm 1$. In this case, both the classical motion of the center of mass and the quantum dynamics are unstable, and the fidelity decreases rapidly with time with the maximum Lyapunov exponent ($\lambda \approx 0.04$ for the chosen parameters and initial conditions), which is a classical measure of dynamical chaos (see the thin and thick solid lines in Fig. 3 for $\Delta\delta = 10^{-4}$).

Thus, we have shown that the existence of one classical degree of freedom, which naturally appears in the basic model of cavity QED and is dynamically coupled with quantum degrees of freedom, is sufficient for the appearing complex quantum dynamics including instability and dynamical chaos. This behavior does not require the presence of an infinite reservoir simulating

the environment and/or noise induced by weak continuous measurements. It has been shown that the quantum instability is quantitatively characterized by the maximum Lyapunov exponent, which ensures the quantum–classical correspondence in the basic model of cavity QED.

This work was supported by the Presidium of the Far East Division of the Russian Academy of Sciences and the Presidium of the Russian Academy of Sciences Program “Mathematical Methods in Nonlinear Dynamics.”

REFERENCES

1. B. V. Chirikov, *Chaos* **1**, 95 (1991).
2. W. H. Zurek, *Rev. Mod. Phys.* **75**, 715 (2003).
3. E. Joos, H. D. Zeh, C. Kiefer, D. Giulini, J. Kupsch, and I.-O. Stamatescu, *Decoherence and the Appearance of a Classical World in Quantum Theory*, 2nd ed. (Springer, New York, 2003).
4. S. Ghose, P. Alsing, I. Deutsch, *et al.*, *Phys. Rev. A* **67**, 052102 (2003).
5. H. Carmichael, *An Open System Approach to Quantum Optics* (Springer, Berlin, 1993).
6. A. Peres, *Phys. Rev. A* **30**, 1610 (1984).
7. P. Horak, H. Ritsh, T. Fischer, *et al.*, *Phys. Rev. Lett.* **88**, 043601 (2002); T. W. Lynn, K. Birnbaum, and H. J. Kimble, *quant-ph/0507064* (2005); S. Husmann *et al.*, *quant-ph/0506088* (2005).
8. S. V. Prants, *Vestn. Dal’nevost. Otd. Ross. Akad. Nauk*, No. 2, 30 (2003).
9. S. V. Prants and M. Yu. Uleysky, *Phys. Lett. A* **309**, 357 (2003).
10. M. Yu. Uleysky, L. E. Kon’kov, and S. V. Prants, *Commun. Nonlinear Sci. Numer. Simul.* **8**, 329 (2003).
11. S. V. Prants, *Pis’ma Zh. Éksp. Teor. Fiz.* **75**, 71 (2002) [*JETP Lett.* **75**, 63 (2002)].
12. V. Yu. Argonov and S. V. Prants, *Zh. Éksp. Teor. Fiz.* **123**, 946 (2003) [*JETP* **96**, 832 (2003)].

Translated by R. Tyapaev

Generation of Terahertz Radiation upon the Optical Breakdown of a Gas

A. M. Bystrov, N. V. Vvedenskii, and V. B. Gildenburg*

Institute of Applied Physics, Russian Academy of Sciences, ul. Ul'yanova 46, Nizhni Novgorod, 603950 Russia

* e-mail: gil@appl.sci-nnov.ru

Received September 26, 2005; in final form, November 2, 2005

Terahertz radiation of plasma oscillations excited upon the optical (axicon) breakdown of a gas in the presence of external fields of other frequency ranges has been analyzed. It has been shown that the spectra and intensity of oscillations and radiation generated by them depend strongly on the character of the spatiotemporal evolution of the formed plasma. The intensity is maximal upon the rapid formation of the plasma with a sharp boundary and decreases to very low values for objects with a smooth density profile. New schemes and regimes of breakdown have been proposed, which make possible, according to preliminary estimates, an emitted energy of about 10 mJ with moderate intensities of ionizing laser radiation. © 2005 Pleiades Publishing, Inc.

PACS numbers: 52.35.-g, 52.38.-r, 52.59.Ye

1. As is known, the breakdown of a medium by intense laser pulses may be accompanied by the generation of natural oscillations and waves in the formed plasma. Two different physical mechanisms of this phenomenon are known. The first mechanism is associated with the action of the averaged ponderomotive force on free electrons that excites free Langmuir waves in the wake of a laser pulse. The longitudinal fields of these waves can accelerate electrons synchronized with them to high energies. Owing to this property, this mechanism is used in laser-plasma methods actively developed in recent years for accelerating charged particles [1]. The other mechanism of the excitation of natural oscillations and waves is quite well known but is less studied and directly associated with an increase in the plasma density and the corresponding rearrangement of the wave mode spectrum in the ionized region of the medium in the process of optical breakdown [2–7]. In contrast to the first mechanism that is nonlinear in physical nature, the second mechanism is linear in essence and, therefore, ensures much more efficient transformation of the energy of moderately intense pumping fields to the energy of free oscillations. Both the ionizing radiation itself [3, 4] and the extraneous fields of other frequency ranges (including static fields) [2, 5–7] can serve as pumping that ensures the energy of excited oscillations in this mechanism. Since a considerable fraction of the energy of oscillations can be reemitted coherently to the environment and their frequencies can be controlled over a wide range by varying the parameters of the ionized medium (e.g., gas pressure), this mechanism seems to be promising as a tool for generating electromagnetic radiation in certain, hardly accessible, frequency ranges (terahertz, soft x-ray). In particular, the authors of [5–7] studied both theoretically and

experimentally various schemes of generating terahertz radiation arising upon the optical breakdown of a gas in the presence of static electric fields. They considered breakdown induced by a beam focused in the spacing between the plates of a charged plane capacitor [6], as well as fast ionization waves in the focal region of a cylindrical lens (in a spatially periodic electric field) [5] and on the axis of a Bessel beam formed by an axicon lens (in a uniform electric field) [7].

The results obtained demonstrate the principle possibility of using the parametric transformation of fields upon the breakdown of the medium to generate terahertz radiation. However, those investigations cannot enable one to calculate the real efficiency of such a transformation and to indicate (at least qualitative) optimum conditions for its realization, because they ignored important problems concerning the dependence of the intensity of the excited oscillations and the corresponding radiation on the character of the spatiotemporal evolution of the plasma in the breakdown process. In the theoretical models [2, 5, 7], only a homogeneous plasma with a sharp boundary was considered and the breakdown time interval was assumed to be negligibly small. The aim of this work is to analyze the processes of the transformation of external fields (both static and varying) to the fields of the natural oscillations of the plasma that is formed upon gas breakdown with allowance for its real inhomogeneity, the nonzero time interval of its formation, and the radiative damping of excited plasma oscillations that was previously ignored. As will be shown, the inclusion of these factors can significantly change the pattern of the phenomenon under consideration. In particular, a smooth density gradient in the boundary layer of the plasma results in the strong additional broadening of

the spectrum of excited natural oscillations and suppression of their emitting component (even under the conditions of instantaneous gas ionization).

2. For the generation scheme [7] involving the generation of a fast transverse polarization wave that is excited behind the front of a superlight breakdown wave in a narrow near-axial region of the axicon lens, we primarily analyze the natural quasi-electrostatic oscillations (with frequencies on the order of the maximum plasma frequency ω_{p0}) generated in the presence of a given external electric field (varying or constant) in the time-varying cylindrically symmetric plasma. The plasma is created by a short laser pulse (with the duration $\tau_p \sim 100$ fs) focused by a conic lens (axicon) into a so-called Bessel wave beam propagating without divergence along the symmetry axis z at the distance $\Delta z = L$, which depends on the wave-beam radius b at the entrance of the lens and the angle ϑ_0 between the rays passed through it and the axis (in particular, $\vartheta_0 \sim 0.1$, $b \sim 1$ cm, and $L \sim b/\sin\vartheta_0 \sim 10$ cm in experiments [8]). The velocity of the ionization wave created by the laser pulse in the segment Δz is equal to the phase velocity of the light wave $V_i = c/\cos\vartheta_0 > c$. A given external field $\mathbf{E}_0 = \mathbf{e}_x E_{0x}$ (perpendicular to the z axis in the scheme under consideration) either is uniform and constant (as was assumed in [7]) or is a wave with frequency ω_0 that propagates with phase velocity V_0 along the z axis

$$E_{0x} = E_0 \cos(\omega_0 t - h_0 z), \quad h_0 = \omega_0/V_0. \quad (1)$$

In the latter case, we really suppose that the ionizing laser pulse is introduced into an open or closed waveguide directing a wave of a certain type. The frequencies ω_{p0} and ω_0 , characteristic ionization time τ_i , and the radius a of a formed plasma cylinder for the case of interest satisfy the conditions $\omega_0 \tau_i \ll 1$, $\omega_0 \ll \omega_{p0}$, $a \ll L$, $h_0 a \ll 1$, and $a \omega_{p0} \ll c$, which make it possible to calculate perturbations of the field and the electron density in each given cross section $z = \text{const}$ by solving the two-dimensional quasi-electrostatic problem on the potential oscillations of the radially inhomogeneous nonstationary plasma in the external transverse field \mathbf{E}_0 and to perform this calculation by disregarding the transverse inhomogeneity of both this field and the plasma cylinder created in it. In this approach, the longitudinal coordinate z appears in the solution only as a parameter determining the beginning of the breakdown time $t_b = z/V_i$ and the external-field phase at this time $\phi_b = \omega_0 t_b - h_0 z$. In addition, the plasma density (in fact, ion density) $N(r, \tau)$, which is completely determined by the dynamics of the optical breakdown, is a function of the distance r from the axis and delaying time $\tau = t - t_b$.

The character of the joint spatiotemporal evolution of the optical field and plasma in axicon breakdown depends strongly on the ratio between the concentration N_g of the neutral molecules of the gas, which determines the plasma density maximum N_{\max} , and the den-

sity $N_1 = N_{cL} \sin^2 \vartheta_0$ corresponding to the total reflection of the optical radiation ($N_{cL} = m \omega_L^2 / 4\pi e^2$ is the critical concentration for the optical frequency ω_L). According to the calculation based on the solution of the corresponding self-consistent problem [4], two substantially different scenarios of the process under consideration are possible for the moderate parameters of ionizing laser pulses (which have been obtained in many laboratories) that we consider in this work (the intensity $I \sim 10^{14} - 10^{15}$ W/cm², and $\tau_p \sim 100$ fs). In the first scenario realized when the formed plasma strongly screens the radiation ($N_g > N_1$), the radial density profile $N(r)$ is bell-shaped at all stages (with a maximum on the axis equal or close to N_g) and is characterized by a certain unified scale $a(\tau)$. The second scenario is realized when the plasma slightly perturbs the optical field ($N_g \ll N_1$), even upon the complete (single) ionization of the gas. In this case, the breakdown process occurs in two stages. At the first stage, which completes at the time of the complete ionization of the gas on the axis, the process occurs through the first scenario (the radial profile remains single-scale). At the second stage, a continuously expanding region of the homogeneous plasma with $N = N_g$ [the plateau of the radius $r = R(\tau)$ on the density profile] appears near the axis. At the end of this stage, both characteristic sizes (the outer radius a and the plateau radius R) are determined by the transverse size of the Bessel beam ($a \sim R \sim c/\omega_L \sin\vartheta_0$) and their difference (the width of the transition boundary region) is $a - R \sim (0.2 - 0.3)a$.

3. The interaction of the formed inhomogeneous plasma with the external field \mathbf{E}_0 in the approximation under consideration can be described by the system of equations for the volume charge density ρ and self-consistent field potential $\mathbf{E} = -\nabla\phi(\mathbf{r}, \tau)$:

$$\frac{\partial^2 \rho}{\partial \tau^2} + v \frac{\partial \rho}{\partial \tau} + \omega_p^2 \rho = \frac{1}{4\pi} \nabla \omega_p^2 \nabla \phi; \quad (2)$$

$$\Delta \phi = -4\pi \rho.$$

Here, $\omega_p^2(r, \tau) = 4\pi e^2 N(r, \tau)/m$, and v is the effective collision frequency between electrons and heavy particles. The first of Eqs. (2) is easily derived from the charge conservation law and the equation for the electron current density $\partial \mathbf{j} / \partial \tau + \mathbf{v} \mathbf{j} = (\omega_p^2 / 4\pi) \mathbf{E}$, which is valid for any variation rate for the plasma density N in the breakdown process [3, 4]. In view of the assumed uniformity of the external field, we are interested in the dipole-type solution for which the field potential outside the plasma is the sum of the potentials of the given external field and the field of a two-dimensional (linear) electric dipole with the dipole-moment density per unit length $P = \iint \rho x ds$ (the integral is calculated over the cross section of the cylinder). As follows from the boundedness of the function $\phi(\mathbf{r}, \tau)$ at $r = 0$ and the con-

tinuity of the field and the potential at $r = a$, this function satisfies the boundary conditions $\varphi(0, \tau) = 0$ and $(\partial\varphi/\partial r)_{r=a} + \varphi(a)/a = -2E_{0x}/r$.

For a uniform cylinder with a sharp boundary ($\omega_p(r < a) = \omega_{p0} = \text{const}$), it is easy to show that the charge is located on the plasma surface [$\rho \sim \delta(r - a)$] and the dipole moment satisfies the known equation

$$\ddot{P} + \nu\dot{P} + \omega_c^2 P = (\omega_c^2/2)a^2 E_{0x}, \quad (3)$$

where the frequency $\omega_c = \omega_{p0}/\sqrt{2}$ of the so-called geometric resonance of the cylinder and the external field E_{0x} can be treated as given arbitrary functions of time. As was shown in [9, 10], the oscillatory properties of a plasma object with smooth density distributions strongly differ from those for stepwise distributions. The spectrum of the plasma oscillations becomes continuous, because their frequency $\omega_p(r)$ is a function of coordinates [10] and the geometric resonance weakens strongly due to resonance absorption at $N \approx N_c = m\omega_c^2/4\pi e^2$ [9].

In order to describe the oscillatory processes in the inhomogeneous nonstationary plasma formed under the conditions of the optical breakdown of the gas, Eqs. (2) with the above boundary conditions and with the zero initial conditions $\rho = \partial\rho/\partial\tau = 0$ corresponding to the problem formulated above at $\tau = 0$ are integrated numerically. The spatiotemporal density distributions $N(r, \tau)$ simulating the breakdown scenarios described above are approximated by certain simple piecewise analytic functions. As the basic parameters entering into the definition of these functions (which are not given here, because they are comparatively lengthy), we specify the maximum density $N_{\text{max}} = N_g$, the time of reaching the steady state (characteristic ionization time) τ_i , and the structure parameters of this state—the ionized-region radius a and plateau radius R (which is nonzero only for the second scenario). In view of the accepted conditions $\omega_0\tau_i \ll 1$ and $\omega_0 \ll \omega_{p0}$, the external field was assumed to be constant (independent of τ) in the calculations: $E_{0x} = E_0 \cos\phi_b$.

Calculation results are shown in Figs. 1–3. Figure 1 shows the time dependences of the dipole moment per unit length $p(\tau)$ normalized to its stationary value $P_b = a^2 E_{0x}/2$. For small values of the ratio ν/ω_c , the damping rate and amplitude of the dipole oscillations accompanying the transition from the initial state with $P = 0$ to the final state with $P = P_b$ depend strongly on the diffusion of the plasma boundary (determined by the parameter R/a) and the dimensionless ionization time $\omega_{p0}\tau_i$. In the absence of the plateau, the oscillations are very small and rapidly damped even for the case of instantaneous ionization (Fig. 1a); as the ratio R/a increases, the amplitude of the oscillations increases and their damping rate decreases (Fig. 1b). An increase in the ionization time τ_i noticeably reduces the amplitude of the excited oscillations beginning with the parameter

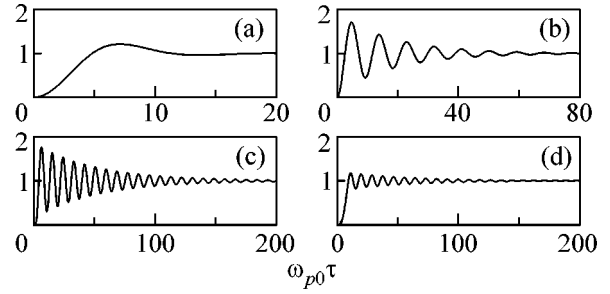


Fig. 1. Time dependences of the dipole moment $p(\tau) = P(\tau)/P_0$ at $\nu/\omega_c = 5 \times 10^{-3}$ for (a) $R/a = 0$ and $\omega_{p0}\tau_i = 0$, (b) $R/a = 0.75$ and $\omega_{p0}\tau_i = 0$, (c) $R/a = 0.9$ and $\omega_{p0}\tau_i = 3$, and (d) $R/a = 0.9$ and $\omega_{p0}\tau_i = 10$.

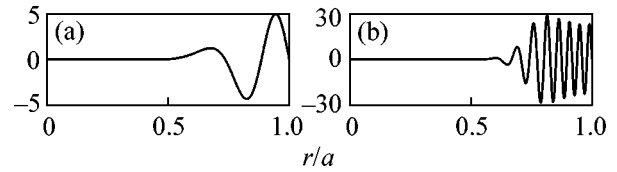


Fig. 2. Radial profiles of the charge density $\rho a/E_{0x}$ on the x axis at $\nu/\omega_c = 5 \times 10^{-3}$, $\tau_i = 0$, and $R/a = 0.5$ for $\omega_{p0}\tau =$ (a) 10 and (b) 50.

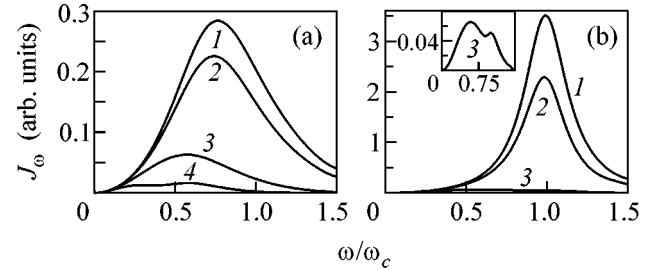


Fig. 3. Radiation spectra J_ω at $\nu/\omega_c = 5 \times 10^{-2}$ for (a) $R/a = 0$ and $\omega_{p0}\tau_i = (1) 0, (2) 3, (3) 10,$ and $(4) 20$ and for (b) $R/a = 0.6$ and $\omega_{p0}\tau_i = (1) 0, (2) 3,$ and $(3) 10$.

$\omega_{p0}\tau_i \approx 3$; the amplitude for $\omega_{p0}\tau_i = 10$ and $R \approx a$ is about one fifth of the value for $\tau_i = 0$ (see Figs. 1c and 1d).

Strong damping of the natural dipole oscillations of the plasma cylinder with a smooth radial density profile for low collision frequencies can be interpreted as the manifestation of a certain additional (collisionless) mechanism of dissipation associated with the transformation of the energy of the large-scale component of the field and plasma polarization to the small-scale component that does not contribute to the dipole moment. This process of the accumulation of the energy of the small-scale component, which is finally due to the continuous increase in the gradient of the

plasma-oscillation phase $\omega_p(r)\tau$ with time, is illustrated in Fig. 2, where the spatial charge density distributions $\rho(r)$ are shown for various times. We emphasize that the continuous decrease in the spatial scale of the oscillations under real conditions ceases at a certain time due to the onset of actual dissipation (e.g., Landau damping that is ignored here); however, this circumstance is already immaterial for describing the dipole oscillations of interest.

4. In order to describe the radiation generated by natural dipole oscillations, we calculate the Fourier spectra of the second derivative of the dipole moment. Figure 3 shows the frequency dependences of the quantity $J_\omega = |(d^2p/d\tau^2)_\omega|^2$, which determines the spectral intensity of the radiation in the principal-maximum direction. As is seen, for small v/ω values, the linewidth $\Delta\omega$ (determined by the internal energy losses considered above) increases both as the ratio R/a decreases and as $\omega_{p0}\tau_i$ increases. In this case, the maximum radiation intensity $J_{\omega_{\max}}$ can decrease by several orders of magnitude.

For the case of fast ionization and low internal losses (i.e., for $v \ll \omega_c$, $R \approx a$, and $\omega_{p0}\tau_i < 1$), which is of most practical interest, the solution of system (2) can be found analytically using the Laplace transform. The time dependence of the dipole moment that corresponds to this (approximate) solution is described by the function

$$P = P_b[1 - \cos(\omega_c\tau)\exp(-\gamma_i\tau)]\theta(\tau), \quad (4)$$

where $\gamma_i = v/2 + \omega_c l/a$, $l = |N/\nabla N|_{N=N_c} \ll a$, $\theta(\tau < 0) = 0$, and $\theta(\tau > 0) = 1$. Dependence (4) agrees well with the above numerical calculation ($\gamma_i \approx \Delta\omega/2$) for $l \ll a$ and can also be used in approximate estimates at $l \sim a$. In view of Eq. (1), the varying polarization component P_- determined by function (4) can be represented as the superposition of two damping waves (excited in the interval $0 < z < L$ behind the moving ionization front) with the frequency ω_c and different longitudinal wavenumbers:

$$P_- = \frac{P_0}{2}[\cos(\omega_c t - h_1 z) + \cos(\omega_c t - h_2 z)] \times \exp(-\gamma_i\tau)\theta(\tau), \quad (5)$$

where $P_0 = a^2 E_0/2$ and $h_{1,2} = \omega_c V_i^{-1} \pm \omega_0(V_i^{-1} - V_0^{-1})$. Since these waves are fast under the conditions on hand ($V_{1,2} = \omega_c/h_{1,2} > c$), each of them emits in the directions forming the angles $\vartheta_{1,2} = \arccos(c/V_{1,2})$ with the z axis and the angular width of the emission maxima is $\Delta\vartheta_{1,2} \approx c/\omega_c L \sin\vartheta_{1,2}$. As is easily shown by calculating the electromagnetic field in the far zone of the linear radiator of the length $L \gg c/\omega_c$ under consideration and generalizing Eqs. (4) and (5) with the inclusion of radiative losses, the total power Π and energy W of radia-

tion for the case of weak damping and fast ionization are given by the expressions

$$\Pi = \frac{\pi\omega_c^3}{4c^2} P_0^2 L \exp(-2\gamma t), \quad W = \int_0^\infty \Pi dt = W_0 \frac{\gamma_r}{\gamma}. \quad (6)$$

Here, $\gamma_r = \pi\omega_c^3 a^2/8c^2$ is the radiative damping constant, $W_0 = P_0 E_0 L/2$ is the energy of the electrostatic dipole interaction between the external field and the plasma, and $\gamma = (v/2) + \omega_c l/a + \gamma_r$ is the total linewidth including internal and radiative losses. For nonzero $\omega_{p0}\tau_i$ values, a correcting factor $\mu < 1$ depending on the parameters R/a and $\omega_{p0}\tau_i$ should be introduced into expressions (6) and its value can be determined by using the plots in Figs. 1 and 3.

5. The above results enable one to approximately evaluate the power and energy of radiation in various breakdown regimes and to indicate the optimum conditions for realizing the mechanism considered for generating terahertz radiation. In particular, for the parameter values accepted in [7] (the air pressure $p = 1$ atm, the external static field $E_0 = 30$ kV/cm, the frequency $f_c = \omega_c/2\pi = 30$ THz, the plasma-cylinder sizes $a = 2$ μm and $L = 1$ cm, the focusing angle $\vartheta_0 \approx 0.1$, and the collision frequency $\nu = 10^{13}$ 1/s) and using data from [4], we obtain $\omega_{p0}\tau_i \approx 20$ and $R = 0$ (the first breakdown scenario is realized). As follows from the plots in Figs. 1 and 3, a large $\omega_{p0}\tau_i$ value and the absence of a sharp density gradient at the boundary strongly reduce the amplitude of the oscillations and the intensity of the radiation. The energy emitted in this case is $W \approx 3 \times 10^{-2} W_0 \approx 3 \times 10^{-13}$ J (rather than the value of 10^{-10} J obtained in [7] disregarding the radiative damping of the oscillations under the assumption of instantaneous homogeneous ionization).

In the above example, the external field E_0 was taken to be equal to the threshold field of the static breakdown of air $E_{\text{th}}(\text{kV/cm}) = 30p(\text{atm})$. This threshold can be increased in alternating fields for which $E_{\text{th}} \approx 30p\sqrt{1 + (20p\lambda_0)^{-2}}$ (in the same units), where $\lambda_0(\text{cm}) = 2\pi c/\omega_0$. In this case, the gas density can decrease to $N_g < N_{cL} \sin^2\vartheta_0$, at which the axicon breakdown regime can be realized with $\omega_{p0}\tau_i \sim 1$ and $l \ll a$. In addition, the parameters of the plasma and the radiation generated by it depend strongly on the angle ϑ_0 , the beam radius b on the lens, and the wavelengths λ_0 and $\lambda_c = 2\pi c/\omega_c = 10^{-3}/\sqrt{p}$ (atm). The emitted energy is maximal near the boundary of the region of the quasistatic description ($\omega_c a/c \approx \omega_c/\omega_L \vartheta_0 = \sqrt{N_g/2N_{cL}} \vartheta_0^{-1} \approx 0.5$), where the optimum angle is $\vartheta_0 \approx 1.6 \times 10^{-4}/\lambda_c$, $\omega_{p0}\tau_i < 3$, $l/a \approx 0.1$, $\gamma_r \approx \gamma/2 \approx 0.1\omega_c$, $\Pi(W) \approx 10^6(\lambda_c/\lambda_0)^2 b$, and $W(\text{J}) \approx 10^{-5} b \lambda_c^3/\lambda_0^2$ (λ_c , λ_0 , and b are measured in centimeters) in a wide wavelength range

($6 \times 10^{-3} \text{ cm} < \lambda_c < \lambda_0 < 2 \text{ cm}$) for the parameters realized in the experiment described in [8] ($\lambda_L \approx 0.8 \text{ }\mu\text{m}$, $I \sim 10^{14} \text{ W/cm}^2$, and $\tau_p \sim 100 \text{ fs}$). In particular, a radiation pulse with $\lambda_c \sim 10^{-2} \text{ cm}$ (central spectral frequency $f_c = 3 \text{ THz}$), power $\Pi \approx 40 \text{ kW}$, and energy $W \approx 4 \text{ nJ}$ is generated for $\lambda_0 = 0.1 \text{ cm}$ and $p = 10^{-2} \text{ atm}$ at the parameters $b = 4 \text{ cm}$ and $\vartheta_0 = 1^\circ$ realized in the experiments reported in [11].

A significant increase in energy can likely be achieved by removing the constraint $E_0 < E_{\text{th}}$. In this case, fast optical breakdown can occur against the background of a slower ionization process initiated by pulses of the external field $E_0(t)$ exciting natural oscillations. If the time $t = t_b$ of introducing a femtosecond laser pulse is well synchronized with the time of reaching the maximum excited field [$E_0(t_b) = E_{0\text{max}}$] and the plasma at this time is not too dense ($N < N_{c0} = m\omega_0^2/4\pi e^2$), the amplitude of excited oscillations and emitted energy are determined by the quantity $E_{0\text{max}}$. In particular, such a situation may be realized at an air pressure of $p = 10^{-3} \text{ atm}$ (corresponding to the radiation frequency $f_c = 1 \text{ THz}$) and at the parameters of exciting microwave pulses achieved at present in the accelerating systems of electron–positron colliders [12] ($\lambda_0 = 1 \text{ cm}$, duration $\sim 3 \text{ ns}$ of the leading front of a pulse, and $E_{0\text{max}} \approx 4 \times 10^6 \text{ V/cm}$). Under these conditions, we obtain $W \approx 10 \text{ mJ}$ at the small angle $\vartheta_0 = 20'$ for the parameters $b = 4 \text{ cm}$ and $I \sim 10^{14} \text{ W/cm}^2$. This preliminary estimate shows that the generation method under consideration with the use of pulsed exciting fields can ensure emitted energies that are much higher than both the experimentally measured ($< 100 \text{ nJ}$) and theoretically predicted ($100 \text{ }\mu\text{J}$) values reached in laser–plasma systems in which the mechanism of the ponderomotive excitation of plasma oscillations and acceleration of electron bunches in intense beams ($\sim 10^{19} \text{ W/cm}^2$) is used [13].

This work was supported by the Russian Foundation for Basic Research (project no. 04-02-16684) and the Russian Science Support Foundation.

REFERENCES

1. T. Katsouleas, *Nature* **431**, 515 (2004).
2. S. C. Wilks, J. M. Dawson, and W. B. Mori, *Phys. Rev. Lett.* **61**, 337 (1988); M. I. Bakunov and A. V. Maslov, *Phys. Rev. Lett.* **79**, 4585 (1997); C. H. Lai, R. Liou, T. C. Katsouleas, *et al.*, *Phys. Rev. Lett.* **77**, 4764 (1996); V. B. Gildenburg and N. V. Vvedenskii, *Probl. At. Sci. Technol., Ser.: Plasma Phys.* **11**, 110 (2005).
3. V. B. Gildenburg, A. G. Litvak, and N. A. Zharova, *Phys. Rev. Lett.* **78**, 2968 (1997); M. I. Bakunov, A. M. Bystrov, and V. B. Gildenburg, *Phys. Plasmas* **9**, 2803 (2002).
4. N. V. Vvedenskii and V. B. Gildenburg, *Pis'ma Zh. Éksp. Teor. Fiz.* **76**, 440 (2002) [*JETP Lett.* **76**, 380 (2002)].
5. D. Hashimshony, A. Zigler, and K. Papadopoulos, *Phys. Rev. Lett.* **86**, 2806 (2001).
6. T. Löffler and H. G. Roskos, *J. Appl. Phys.* **91**, 2611 (2002).
7. S. V. Golubev, E. V. Suvorov, and A. G. Shalashov, *Pis'ma Zh. Éksp. Teor. Fiz.* **79**, 443 (2004) [*JETP Lett.* **79**, 361 (2004)].
8. A. A. Babin, A. M. Kiselev, D. I. Kulagin, *et al.*, *Pis'ma Zh. Éksp. Teor. Fiz.* **80**, 344 (2004) [*JETP Lett.* **80**, 298 (2004)].
9. V. B. Gildenburg, *Zh. Éksp. Teor. Fiz.* **45**, 1978 (1963) [*Sov. Phys. JETP* **18**, 1358 (1963)].
10. E. M. Barston, *Ann. Phys. (N.Y.)* **29**, 282 (1964); B. B. Kadomtsev, *Collective Phenomena in a Plasma* (Nauka, Moscow, 1988) [in Russian].
11. S. S. Bychkov, S. V. Gorlov, A. V. Makarov, *et al.*, *Kvantovaya Élektron. (Moscow)* **26**, 243 (1999).
12. H. H. Braun, S. Döbert, I. Wilson, and W. Wuensch, *Phys. Rev. Lett.* **90**, 224801 (2003).
13. W. P. Leemans, J. van Tilborg, J. Faure, *et al.*, *Phys. Plasmas* **11**, 2899 (2004).

Translated by R. Tyapaev

Wake-Induced Symmetry-Breaking of Dust Particle Arrangements in a Complex Plasma[†]

A. A. Samarian, S. V. Vladimirov, and B. W. James

School of Physics, The University of Sydney, New South Wales 2006, Australia

Received October 21, 2005; in final form, November 9, 2005

A symmetry-breaking disruption occurs in a system of two dust particles with a decrease of the particle separation. This disruption is attributed to the formation of the common ion wake in the system. In the experiment, the particles levitate in the sheath of a radio-frequency (rf) discharge at low gas pressures (≤ 60 mTorr) and their separation is changed by the laser manipulation. The experiment is complemented by molecular dynamics (MD) numerical simulations. The experimental and simulation data agree that the disruption condition corresponds to the common ion wake formation at the interparticle distances less than the electron Debye length.
© 2005 Pleiades Publishing, Inc.

PACS numbers: 52.27.Lw, 52.35.Py, 52.80.Pi

The complex plasmas, i.e., plasmas containing solid mesoscopic particles (“dust” particles, larger as compared with the sizes of ions and neutral atoms but less than the typical collective plasma scales such as the Debye length), recently appear to be useful and convenient objects to model numerous fundamental physical phenomena such as phase transitions, diffusion and transport, and symmetry breaking [1, 2]. The ability to study phenomena at the individual particle level allows researchers to directly investigate the kinetics of many fundamental phenomena previously attributed mainly to condensed matter physics.

The dust particles in a complex plasma tend to self-organize themselves in various ordered structures such as dust crystals, strings, and clusters [3, 4]. In a typical experiment [3, 4], the dust structures levitate in the sheath region, where the strong ion flow to the electrode is established. The ion flow naturally provides a distinctive direction and reduces the symmetry of the considered system. This is responsible for the vertically aligned crystal structure and string formation.

The nature of the particle alignments in systems containing a large number of particles can be understood by considering simplified systems of just a few (e.g., two) particles [4–9], thus, allowing us to elucidate the physics of the reduced symmetry in dust-plasma structures. One of the major factors that affect the symmetry of the dust arrangements in discharge plasma is the ion wake formed downstream from the particles in the presence of an ion flow, as demonstrated theoretically, experimentally, and numerically [10–15]. With this reasoning, the dust particles behave as Cooper-like pairs and the plasma polarization in the ion focus leads to the appearance of the “binding” force that is respon-

sible, e.g., for the formation of dust molecules [4, 11]. Thus, the wake changes the symmetry of the particle interaction, and, therefore, the symmetry of the dust structures.

It is well known that the symmetry breaking occurs if a system allows an asymmetric stable state when a controlling parameter (such as an order parameter) reaches a certain value [16]. One of the striking observations of the symmetry breaking in a complex plasma was the disruption in the two particle system where the particles changed their arrangement from the horizontal to the vertical one depending on the discharge parameters (pressure or input rf power). It was pointed out that the state of the system is determined by the values of the particle coupling energy and the energy of the horizontal and vertical confinements, as well as by the influence of the wake potential [6]. Later, the effect of the horizontal and vertical confinements on the stability of the particle arrangements was analytically considered in [7]. The further elucidation of the role of the horizontal and vertical confinements was done in the experiment [9] where the symmetry breaking was triggered by applying an additional bias voltage to change the confinements' ratio.

The symmetry breaking in the two particle system generally appears as an initially continuous change of the position of one particle going closer and below another one followed by an abrupt change of the symmetry (the first particle jumps straight below the second particle) at the second (discontinuous) stage. All the previous analyses were concentrated on the first continuous stage. This corresponds to the absence of the bifurcation and allows a simple analytic treatment in terms of the stability of small (linearized) oscillations. The analysis of the second discontinuous stage, as was stressed in [6], is a rather complicated problem requiring under-

[†]The text was submitted by the authors in English.

standing of the ion wake focus characteristics in the presence of the nearby particle and involving the nonlinear wake dynamics that can be adequately treated by numerical simulations—an issue not resolved at that time.

In this letter, we report on experiments on the ion wake-induced symmetry breaking in the two-particle arrangement complemented with molecular dynamics (MD) simulations of the nonlinear ion wake formed in the system of two nearby dust particles. The previous experimental studies [5, 6] where the particle disruptions were triggered by changes in the discharge parameters, i.e., by changes of all the parameters in the systems, make proper comparison with the theory and/or simulations deficient. In our experiments, the disruption was triggered by a laser beam focused on one particle, thus, pushing it closer to another particle. In that case, the change in the particle separation was accompanied by keeping all the other system (plasma) parameters constant, and the discontinuous stage of the symmetry-breaking disruption was induced by only changing the interparticle distance. Note that the laser-assisted manipulation of dust particles was first reported in [11], where the top particles were shifted by a laser beam with the bottom particles following the motions of the top ones. This allowed one to reach a conclusion on the presence of the wake force acting on the bottom particles and to estimate the strength of the wake. A similar experiment was repeated in [5], where the observed hysteresis in the transitions between the particle arrangements (due to the changed discharge parameters such as the gas pressure and the input power) was attributed to the influence of the wake. However, the particle disruption triggered by a laser beam has not yet been reported. Ours is a refined experiment allowing us to exclude all the other possible controlling factors except for the only controlling parameters (the particle separation) and make a direct comparison with the associated numerical simulation. In the simulation, it was observed that a common wake focus of the two nearby particles appears when the particle separation is less than the electron Debye length. This interparticle distance exactly corresponds to that for which the particle jump was observed in the experiment. This allows us to relate the discontinuous stage in the change of the particle arrangement with the formation of the common wake.

In the experiments, monodispersed melamine formaldehyde dust particles with diameters of $2.79 (\pm 0.06 \mu\text{m})$ were introduced into an argon rf discharge. The plasma was generated at pressures in the range 20–60 mTorr, and a 15 MHz signal was applied to the powered electrode. The peak-to-peak voltage measured using an electrical feed through was 25–100 V. The electron temperature, the density, and the plasma potential were measured with an rf-compensated passive Langmuir probe. The electron density was $(2\text{--}9) \times 10^8 \text{ cm}^{-3}$, the electron temperature was about 6 eV, and the plasma potential was 15–65 V.

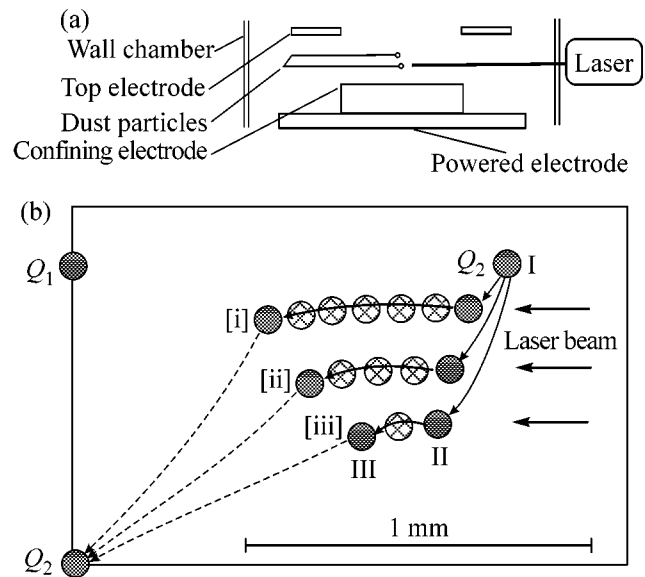


Fig. 1. (a) Experimental setup. Two particles levitate in the sheath of the powered electrode of rf discharge argon plasma. The confinement is provided by the rectangular electrode with a size of 20×7 mm, and the border height is 4 mm. (b) Sketch of the typical laser-induced disruption of the two-particle ($Q_{1,2}$) arrangement; the transition dynamics for three different cases are shown for the neutral gas pressure of 50 mTorr. Transition I–II is induced by the bias (such as 1.2 V for [i], 2.6 V for [ii], and 3.4 V for [iii]) applied by the confining electrode, and transition II–III is induced by the action of the laser. The symmetry breaking disruptions occur at the points III that are different for the particles approaching at the different heights. The jump III–IV (dashed arrows) brings the lower particles to the same position IV below the upper particle.

The experimental set up is shown in Fig. 1a (its details can be found elsewhere [9]). The main difference in the present setup is that the radial confinement is applied by the rectangular electrode placed on the lower electrode. The dc voltage can be applied to the confining electrode in order to change the horizontal confinement. The dust particles were suspended in the plasma using a shaker allowing the release individual particles. The particles were illuminated using a 20 mW Helium–Neon laser. A second (1 W) diode laser was used for the particle manipulation. The diode laser beam was focused on the side particle, and the power of the laser was controlled by the laser diode driver and was varied from 50 mW up to 400 mW. The laser beams enter the discharge chamber through 40 mm diameter windows placed opposite to each other. The observation window, which is mounted on a side port in the perpendicular direction, allows a view of the light scattered at 90° by the suspended dust particles and provides a vertical cross section of the dust particles' arrangement. Images of the illuminated dust particles were obtained using a CCD camera with a 60 mm micro lens and with a digital camcorder (focal length:

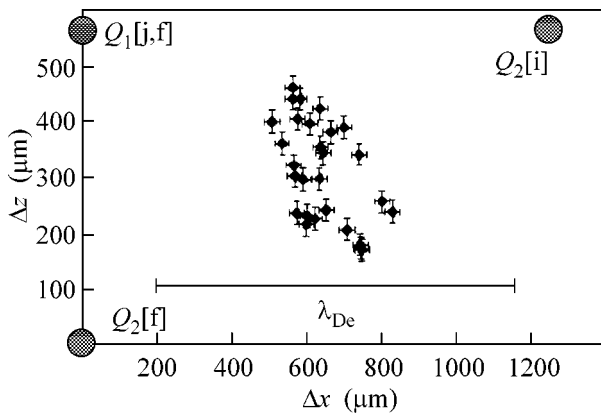


Fig. 2. The experimentally determined disruption points for the two-particle $Q_{1,2}$ system (the neutral gas pressure $P = 30$ mTorr). [i] and [f] stand for the initial and final positions of the particles. The position of the first particle does not change in the transition. The final position of the second particle is always strictly below the first particle. The z axis represents the vertical separation, while the x axis represents the horizontal separation.

5–50 mm). The video signals were transferred to a computer via a frame-grabber card with an 8-bit gray scale and a 640×480 pixel resolution. The coordinates of the particles were measured in each frame, and individual particles were traced from one frame to the next. After the tracking, the data were placed in a spreadsheet and analyzed. From the data analysis, we obtained the particle vertical and horizontal coordinates. The accuracy of the measurement of the particle separation and the levitation height was $30 \mu\text{m}$.

In the experiment, the main goal was to induce the symmetry breaking disruption by only the change of the particle separation, in contrast to all the preceding experiments. Thus, we can single out the effect of the ion wake. The experiment was performed in the following steps. First, we applied a small confining (in the horizontal) bias (up to 5V) to force the initial vertical separation (see Fig. 1b); because of the strong Coulomb repulsion in the horizontal plane, the particles cannot get closer to each other while being at the same height. Second, the lower particle was pushed in the horizontal direction by the diode laser towards the upper particle. The laser power was increased to shift the bottom particle until it jumped directly under the upper one.

The mean interparticle distances for which the symmetry-breaking disruption occurs for different neutral gas pressures

Gas pressure P , mTorr	20	30	40	50	60
Interparticle distance D/λ_{De}	0.77	0.76	0.74	0.72	0.71
Electron Debye length λ_{De} , μm	1021	944	832	657	588

Figure 2 shows the set of the points where the symmetry-breaking disruption occurs for the neutral gas pressure of 30 mTorr. We can see from Fig. 2 that the disruption occurs when the particle separation is less than the electron Debye length. This takes place for various gas discharge pressures. The table gives the average interparticle distance $D = \sqrt{(\Delta x)^2 + (\Delta z)^2}$ (at which the disruption occurs) in the units of the electron Debye length λ_{De} for different gas pressures. The symmetry breaking takes place when the interparticle distance is between $0.7\lambda_{De}$ and $0.8\lambda_{De}$, being almost unchanged for different gas pressures.

The discontinuous nature of the transition demonstrates that some principal change occurs in the system. Since the discharge parameters and confinements are kept constant, we should assume that, with the particle separation decreasing below a certain critical value ($\sim 0.75\lambda_{De}$), the particle–particle and particle–plasma interactions are dramatically changed. The most important factor whose influence can crucially affect the sudden change in the particle interaction is the ion wake focus behind the particles. Here, we relate the symmetry breaking disruption in the particle arrangement with the qualitative change in the wake, that is, to the formation of the common wake of two particles when they are sufficiently close to each other.

To prove this hypothesis, we performed a self-consistent three-dimensional (3D) MD simulation of the kinetics of the plasma electrons and ions around two dust grains shifted with respect to each other. To visualize the ion wake focus, we present the simulated distributions of the ion plasma densities. The details of the numerical technique are described elsewhere [14, 15]. The numerical method involves simulation of the time evolution of the fully ionized ($Z_i = 1$, i.e., the ions are single charged) plasma consisting of N_i positively single-charged ions and N_e negatively charged electrons confined in a simulation box $0 < x < L_x$, $0 < y < L_y$, $0 < z < L_z$, together with the two macroscopic absorbing grains (dust particles), each of diameter $a = 1 \mu\text{m}$, with the infinite masses and the initial (negative) charges $Q_{1,2,0} = Z_{d1,2,0}e = 1000e$, where e is the electron charge. The ions are introduced in the system at the plane $z = 0$ as a uniform flow in the z direction with the Mach number $M = V_0/V_s = 1.41$ and the temperature T_i , where $V_s = (T_e/m_i)^{1/2}$ is the speed of the collisionless sound waves, T_e is the temperature of the plasma electrons (all the temperatures are in energy units, i.e., Boltzmann's constant is unity), and m_i is the ion mass; at $z = L_z$, the ions are removed from the system. The dust particles are placed at $z_1 = L_z/8$; $z_2 = L_z/8 + \Delta z$; and $x_{1,2} = L_x/2 \pm \Delta x/2$; such that Δz , x appear as the distances between them in the direction z parallel to the ion flow and the direction x perpendicular to the flow (the other coordinate of the particles is $y = y_0 = L_y/2$). The equations of motion are solved by the Runge–

Kutta method of the fourth order with the automatically chosen time step. For the characteristic lengths, we have $L_z/3 = L_x/4 = L_y/2 = \lambda_{De}$, where the electron Debye length $\lambda_{De} = 5.256 \mu\text{m}$. The total simulated time of the physical processes is 4.03×10^{-8} s; this should be compared with the ion plasma period $\tau_{pi} = 2\pi/\omega_{pi} = 0.67 \times 10^{-8}$ s.

Figure 3 presents the contour plots of the ion density n_i normalized to $n_{i0} = N_i/L_x L_y L_z$ for $\Delta z = 0.6\lambda_{De}$ and three different distances between the grains. Strong ion focuses are formed behind the dust particles; furthermore, depending on the distance between the particles, the wake maximums are merged at the interparticle distance of $D = \sqrt{(\Delta x)^2 + \Delta z^2} \sim 0.7\lambda_{De}$ (when $\Delta x = 0.4\lambda_{De}$), the case (b), in contrast to their clear separation at the larger interparticle distance ($\Delta x = 0.8\lambda_{De}$), the case (a).

In analogy to the Rayleigh criterion in spectroscopy [17], the beginning of the common wake formation can be determined as the case when the ratio of the ion density between the particles to the mean ion densities behind the particles is 0.7. The common wake is formed in the case when the ion density between the particles exceeds the ion densities behind the particles.

The simulations for the different ion flow velocities were performed, including the case of subsonic ion flow velocities (e.g., $M = 0.8$). The results show that, despite some differences in the ion wake formation for the subsonic and supersonic flows, the common ion wake focus formed behind the particles exhibits the same characteristics depending (crucially) on the particle separation. We also note that the physics of the common wake formation includes complex phenomena of the ion scattering by highly charged macroscopic particles; in particular, the large-angle nonlinear ion scattering in the simplified case of one dust particle and the absence of the flow was investigated only recently [18, 19].

The formation of the common ion wake dramatically changes the particle interaction and the symmetry in the system. This, in turn, has to lead to a drastic change in the particle position. Figure 4 represents the experimentally observed disruption points, along with the results of the MD simulation, which show the area of the common wake formation. The points of the disruption are in very good agreement with the simulation data for the particle separation where the common ion wake is formed. According to Fig. 4, the disruption occurs when the common wake is either starting to form (the gray area between the dashed lines) or has already formed (the ‘‘common wake’’ area below the left dashed line). This figure clearly relates the common wake formation and the disruption in the considered system.

The phenomenon of the common ion wake formation gives a new insight into the ordering of dust particles in the sheath region. It is clear that the adequate description of the state of a many-particle system, as

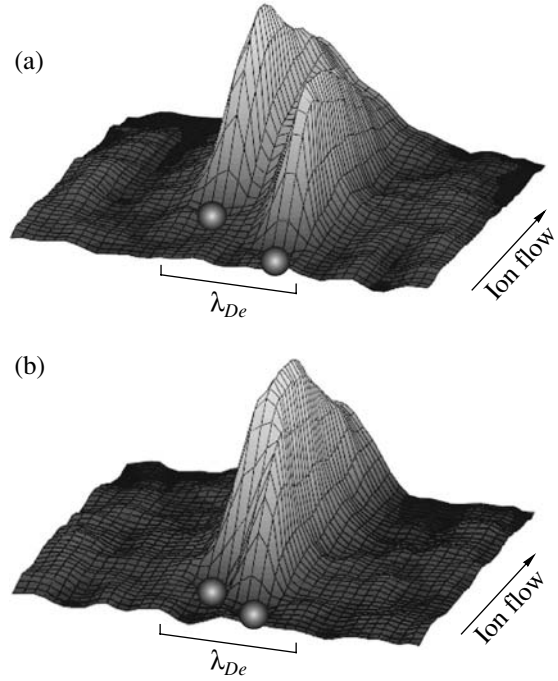


Fig. 3. Surface plots of the MD simulated ion wake focus for the two different separations in the direction x perpendicular to the ion flow: (a) corresponds to $\Delta x = 0.8\lambda_{De}$, and (b) corresponds to $\Delta x = 0.4\lambda_{De}$. Note the formation of the fully developed common wake in case (b).

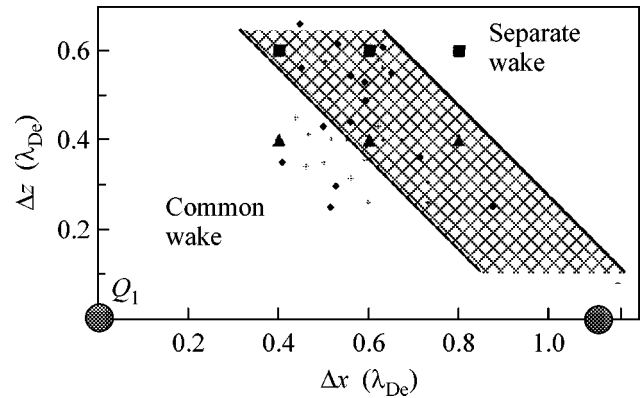


Fig. 4. The symmetry-breaking diagram for the experimentally observed disruption points (the crosses stand for $P = 30$ mTorr and the input power $W = 40$ W, the circles stand for $P = 50$ mTorr and $W = 40$ W, and the diamonds stand for $P = 50$ mTorr and $W = 60$ W). The gray area stands for those particle separations where the common ion wake appears according to the MD simulations.

well as its symmetry and phase transitions, has to include, in addition to the standard linearized (or weakly nonlinear, such as in the perturbation theory) analysis of the dust oscillation characteristics (stable/unstable modes), the influence of the dust particle

separation on the ion focusing including the strongly nonlinear phenomenon of the common wake formation. The discussed symmetry-breaking disruption can be considered as a self-organized transition illustrating the fundamental intrinsic property of a dust structure in a plasma as a self-organized open system. Indeed, by changing the dust-subsystem characteristics, such as the interparticle distance, we inevitably change the ambient plasma characteristics, such as the ion wake focus, which, in turn, can crucially affect the dust subsystem properties (e.g., the positions of the particles) leading to its transition to another ordering state.

The work of A.A.S. was supported by the Denison Fellowship. The work of S.V.V. was supported by the Australian Research Council.

REFERENCES

1. H. Thomas and G. Morfill, *Nature* **379**, 806 (1996).
2. R. L. Merlino and J. A. Goree, *Phys. Today* **57**, 32 (2004).
3. V. E. Fortov *et al.*, *Phys. Usp.* **47**, 447 (2004).
4. S. V. Vladimirov, K. Ostrikov, and A. A. Samarian, *Physics and Applications of Complex Plasmas* (Imperial College, London, 2005).
5. A. Melzer *et al.*, *Phys. Rev. Lett.* **83**, 3194 (1999).
6. V. Steinberg *et al.*, *Phys. Rev. Lett.* **86**, 4540 (2001).
7. S. V. Vladimirov and A. A. Samarian, *Phys. Rev. E* **65**, 046416 (2002).
8. A. M. Ignatov, *Plasma Phys. Rep.* **29**, 296 (2003).
9. A. A. Samarian, S. V. Vladimirov, and B. W. James, *Phys. Plasmas* **12**, 022103 (2005).
10. S. V. Vladimirov and M. Nambu, *Phys. Rev. E* **52**, 2172 (1995).
11. K. Takahashi, T. Oishi, K. Shimonai, *et al.*, *Phys. Rev. E* **58**, 7805 (1998).
12. D. Winske, W. Daughton, D. S. Lemmons, and M. S. Murillo, *Phys. Plasmas* **7**, 2320 (2000).
13. M. Lampe, G. Joyce, and G. Ganguli, *Phys. Plasmas* **7**, 3851 (2000).
14. S. V. Vladimirov, S. A. Maiorov, and N. F. Cramer, *Phys. Rev. E* **67**, 016407 (2003).
15. S. V. Vladimirov, S. A. Maiorov, and O. Ishihara, *Phys. Plasmas* **10**, 3867 (2003).
16. N. Goldenfeld, *Lectures on Phase Transitions and the Renormalization Group* (Addison-Wesley, Reading, Mass., 1992).
17. F. A. Jenkins and H. E. White, *Fundamentals of Optics* (McGraw-Hill, New York, 1976).
18. S. A. Khrapak, A. V. Ivlev, G. E. Morfill, and S. K. Zhdanov, *Phys. Rev. Lett.* **90**, 225002 (2003).
19. S. A. Khrapak, V. N. Tsytovich, A. Ivlev, *et al.*, *Phys. Rev. Lett.* (in press).

Josephson Effect in a Coulomb-Blockaded SINIS Junction[¶]

P. M. Ostrovsky and M. V. Feigel'man

Landau Institute for Theoretical Physics, Russian Academy of Sciences, Moscow, 110334 Russia

e-mail: ostrov@itp.ac.ru

Received November 10, 2005

The problem of a Josephson current through a Coulomb-blocked nanoscale superconductor–normal–superconductor structure with tunnel contacts is reconsidered. Two different contributions to the phase-biased supercurrent $I(\varphi)$ are identified, which are dominant in the limits of weak and strong Coulomb interaction. Full expression for the free energy valid at arbitrary Coulomb strength is found. The current derived from this free energy interpolates between known results for weak and strong Coulomb interaction as the phase bias changes from 0 to π . In the broad range of Coulomb strength, the current–phase relation is substantially nonsinusoidal and qualitatively different from the case of semiballistic SNS junctions. The Coulomb interaction leads to the appearance of a local minimum in the current at some intermediate value of the phase difference applied to the junction. © 2005 Pleiades Publishing, Inc.

PACS numbers: 73.21.–b, 74.45.+c, 74.50.+r

The Josephson current in the contact of two bulk superconductors through a small normal grain (SINIS structure) was recently studied in [1] within the saddle-point approximation for the effective action functional that described [2] superconductive proximity effect in the presence of Coulomb interaction. We found in [1] that Coulomb blockade in the grain results in a very special Josephson current dependence on the phase difference φ (see the dashed lines in Fig. 1). As φ approaches π , the proximity effect in the grain is suppressed, the Coulomb blockade becomes relatively strong, and the spectral minigap induced in the normal grain becomes exponentially small. This led us to the erroneous conclusion that the super-current through the grain is exponentially weak as well. In fact, as was pointed out to us by Beloborodov and Lopatin [3], the supercurrent in the SINIS structure may flow without any spectral minigap at all. The same result was obtained originally by Bruder, Fazio, and Schön in [4] by means of perturbative analysis that is valid as long as the charging energy $E_C = e^2/2C$ is much larger than the proximity-induced minigap (denoted below as \tilde{E}_g). This additional (with respect to our result in [1]) contribution to the supercurrent is due to fluctuational diffusion and Cooperon modes in the N grain, as explained below.

In [1], the replicated dynamical sigma-model was used. The Coulomb interaction in the grain is taken into account in the framework of the adiabatic approximation developed in [2]. The key point of this approximation is the separation of energy scales: the electric potential of the grain fluctuates at a frequency much larger than the proximity induced minigap. This

assumption is valid provided that $E_C \gg \delta$, where δ is the average level spacing in the grain per one spin projection. The saddle point of the sigma-model gives the free energy of the system $F_0(\varphi)$; the current is then calculated using the identity $I_0 = (2e/\hbar)\partial F_0/\partial\varphi$.

The above-mentioned additional contribution to the supercurrent is due to the fluctuations near the saddle point of the sigma model. Below, we present a somewhat more general result used for calculating the fluctuational correction to the total free energy of the system. The supercurrent being the derivative of the free energy with respect to φ acquires significant correction in the regime when the saddle point itself gives an exponentially small result. This, anyhow, happens when the phase difference φ comes close to π . Therefore, the results of [1] and [4] for the Josephson current are, in fact, valid in two limiting cases of weak and strong Coulomb effect, correspondingly.

In order to find the Josephson current in the full range of the Coulomb/proximity ratio, it is necessary to supplement our results presented in [1] by the fluctuational contribution. The saddle-point approximation used in [1, 2] is justified by the inequality $\tilde{E}_g \gg \delta$. The correction due to fluctuations near the saddle point is negligible in this limit. When the phase bias φ is close to π , the parameter \tilde{E}_g becomes exponentially small and the above inequality is violated. It is this violation that makes fluctuational correction important. However, due to the large value of the junction's dimensionless conductance, it is sufficient to consider the fluctuational contribution in the Gaussian approximation not going beyond the quadratic expansion of the action in soft modes. In this paper, we extend the approach of [1, 2] to allow for Gaussian fluctuations near the sigma-

[¶]The text was submitted by the authors in English.

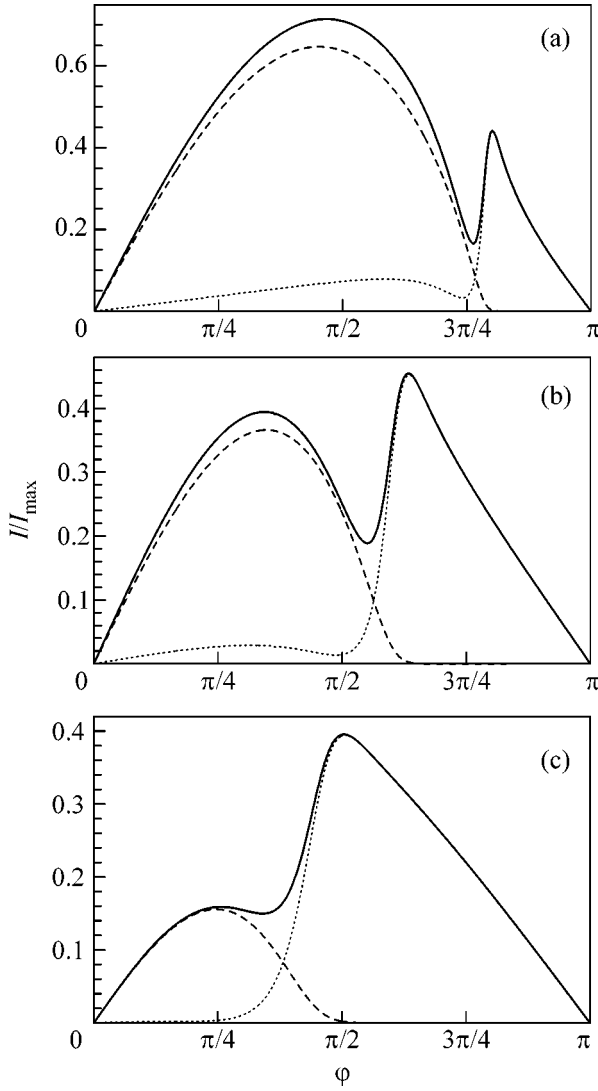


Fig. 1. The dependence of the Josephson current I on phase bias φ . The current is normalized by its maximal value, which is reached at $\varphi = \pi/2$ in the absence of Coulomb interaction $I_{\max} = (e\delta/4\hbar)G_L G_R \log(8\Delta\delta\sqrt{G_L^2 + G_R^2})$. The dashed lines show the dependence (8) found in [1] without fluctuational correction. This correction is depicted by the dotted lines, while the solid curves are the sums of the two contributions. The three plots correspond to the different relative strength of the Coulomb blockade: (a) weak interaction $E_C\delta/E_g^2(0) = 0.5$, (b) intermediate $E_C\delta/E_g^2(0) = 1.5$, (c) strong blockade $E_C\delta/E_g^2(0) = 2.5$. For all three plots, we assume a symmetric junction with $G_L = G_R = 20$ and $\Delta\delta = 3000$. As φ approaches π , the Coulomb interaction always becomes strong and the current is dominated by the fluctuational contribution (29).

model saddle point. The fluctuations are calculated on the background of a non-zero proximity-induced minigap. The resulting dependence $I(\varphi)$ interpolates between that from [1] and that from [4] as φ varies from

0 to π . Moreover, in the crossover region, a local minimum of the supercurrent appears (see Fig. 1). We start with the derivation of the fluctuational contribution to the free energy valid for an arbitrary relative strength of the Coulomb blockade and proximity effect. Then, the current-phase dependence is found by numerical differentiating. To reduce unnecessary complications, the temperature is put to zero. We assume the SINIS junction between two bulk superconductors with tunnel contacts characterized by the large (in e^2/\hbar units) normal conductances G_L and G_R . It is convenient to introduce the effective conductance

$$G(\varphi) = \sqrt{G_L^2 + G_R^2 + 2G_L G_R \cos \varphi}. \quad (1)$$

Formally, one may treat the system as an SIN junction with one superconductive lead and normal conductance given by the above expression [1]. We quantify the proximity effect in the normal grain by the bare value of the induced minigap $E_g(\varphi) = G(\varphi)\delta/4$. This minigap is realized if the Coulomb interaction is absent.

The sigma model for SINIS junction [1, 2] deals with the matrix field $\tilde{Q}_{\varepsilon\varepsilon'}$, which bears two replica and two Matsubara energy (or, equivalently, imaginary time) indices along with a particle-hole structure in Nambu–Gor’kov space. Another field is the scalar phase K_τ^a , which is dependent on the imaginary time and replica number. The action has the form

$$S[\tilde{Q}, K] = -\frac{\pi}{\delta} \text{Tr}(\varepsilon \hat{\tau}_3 \tilde{Q}) + \sum_a \int_0^{1/T} d\tau \left\{ \frac{(\dot{K}_\tau^a)^2}{4E_C} - \frac{\pi}{2} G(\varphi) \text{tr}[\tilde{Q}_{\tau\tau}^{aa}(\hat{\tau}_1 \cos 2K_\tau^a + \hat{\tau}_2 \sin 2K_\tau^a)] \right\}. \quad (2)$$

The symbol $\hat{\tau}_i$ is used for Pauli matrices operating in Nambu–Gor’kov space. The operator Tr implies summation over all indices including the Matsubara energies and replicas, while tr denotes a trace in Nambu–Gor’kov space only.

The adiabatic approximation allows integration out of the field K assuming that \tilde{Q} is fixed. The steady matrix \tilde{Q} is diagonal in energies and trivial in replicas

$$\tilde{Q}_{\varepsilon\varepsilon'}^{ab} = 2\pi\delta^{ab}\delta(\varepsilon - \varepsilon') \frac{\varepsilon \hat{\tau}_3 + \tilde{E}_g \hat{\tau}_1}{\sqrt{\varepsilon^2 + \tilde{E}_g^2}}. \quad (3)$$

Here \tilde{E}_g is the proximity-induced minigap in the normal grain renormalized by the Coulomb interaction. The value of \tilde{E}_g will be determined self-consistently later.

Using the adiabatic approximation, we derive the effective Hamiltonian that determines the dynamics of phase K :

$$H = E_C[-\partial^2/\partial K^2 - 2q \cos 2K], \quad (4)$$

$$q = \frac{E_g(\varphi)\tilde{E}_g}{E_C\delta} \log \frac{2\Delta}{\tilde{E}_g}. \quad (5)$$

The parameter q quantifies the relative strength of the Coulomb blockade [2] in comparison with the proximity effect. In the limit $q \gg 1$, the Coulomb interaction is effectively weak and can be treated perturbatively, while, in the opposite case $q \ll 1$, the Coulomb blockade destroys the proximity effect up to an exponentially small correction. The value of q is determined self-consistently along with \tilde{E}_g .

At zero temperature, K is frozen in the ground state of the Hamiltonian (4) with energy $E_0(q)$. Then, the total free energy acquires the form

$$F_0(\varphi) = -\frac{1}{\delta} \int \frac{\varepsilon^2 d\varepsilon}{\sqrt{\varepsilon^2 + \tilde{E}_g^2}} + E_0(q). \quad (6)$$

The divergent integral is to be regularized by subtracting its value for the ‘‘normal’’ state with $\tilde{E}_g = 0$. In all the subsequent analysis, we assume this regularization to be performed.

The minigap \tilde{E}_g is set by the condition $\partial F_0/\partial \tilde{E}_g = 0$. This gives the self-consistency equation

$$\frac{\tilde{E}_g}{E_g(\varphi)} = -\frac{1}{2E_C} \frac{\partial E_0}{\partial q} = \langle 0 | \cos 2K | 0 \rangle. \quad (7)$$

The last expression implies the average value at the ground state of (4). Together with (5), this equation forms a closed system that determines q and \tilde{E}_g .

In [1], we calculated the supercurrent using the identity $I_0 = (2e/\hbar)\partial F_0/\partial \varphi$. The result was

$$I_0(\varphi) = \frac{e\delta}{4\hbar} \left(\frac{\tilde{E}_g}{E_g}\right)^2 G_L G_R \sin \varphi \log \frac{2\Delta}{\tilde{E}_g}. \quad (8)$$

This dependence of the supercurrent on φ is shown in the Fig. 1 by the dashed lines.

To take into account the fluctuations of \tilde{Q} near the saddle point that was found (for detailed calculations see [5]), we use the parametrization of \tilde{Q} as a rotated $\hat{\tau}_1$ matrix: $\tilde{Q} = V^{-1}e^{-iW/2}\hat{\tau}_1 e^{iW/2}V$. This choice is motivated by the fact that $\tilde{Q} = \hat{\tau}_1$ at $\varepsilon = 0$. Below, we'll see that different modes of fluctuations near the saddle point, diffusions and Cooperons, decouple in this representation. The matrix V diagonal in energies and replicas is determined by the identity $\tilde{Q} = V^{-1}\hat{\tau}_1 V$ and

expressed as $V = \cos(\pi/4 - \theta/2) - i\hat{\tau}_2 \sin(\pi/4 - \theta/2)$ with θ being a standard Usadel angle, and $\tan \theta = \tilde{E}_g/\varepsilon$ dependent on the Matsubara energy. The matrix W describes deviations of \tilde{Q} from the saddle point \tilde{Q} .

W anticommutes with $\hat{\tau}_1$ and, hence, contains two components $W_{\varepsilon\varepsilon'}^{ab} = \hat{\tau}_3 d_{\varepsilon\varepsilon'}^{ab} + \hat{\tau}_2 c_{\varepsilon\varepsilon'}^{ab}$. Below the (off-)diagonal in Nambu space, element $d_{\varepsilon\varepsilon'}^{ab}$ ($c_{\varepsilon\varepsilon'}^{ab}$) is referred to as a diffusion (Cooperon) mode. However, these modes are only analogs of the standard diffusion and Cooperon that describe the fluctuations near the normal metallic saddle point with no minigap.

Now, we substitute the above parameterization into (2) and expand the action to the second order in W . The result is a sum of three terms

$$S[W, K] = S_0[K] + S_1[W, K] + S_2[W, K], \quad (9)$$

where $S_0[K]$ is the action corresponding to the Hamiltonian (4). The terms $S_{1,2}[W, K]$ are linear and quadratic in W respectively; the explicit expressions for them can be found in [5]. Our strategy is to integrate out the phase K . As the fluctuations near the saddle point are assumed to be small, we treat the last two terms of (9) as a perturbation of the bare action $S_0[K]$, or, equivalently, of the Hamiltonian (4). Thus, we expand the statistical weight $e^{-S[W, K]}$ to the second order in S_1 and to the first order in S_2 . Integration with respect to K implies averaging these terms at the ground state of (4). Once the integral is calculated, we rewrite the result in the form of a single exponent

$$\int DWDK e^{-S[W, K]} = e^{-\frac{NF_0}{T}} \int DW e^{-S^{(1)} - S_0^{(2)} - S_{\text{int}}^{(2)}}, \quad (10)$$

$$S^{(1)} = \langle S_1 \rangle, \quad S_0^{(2)} = \langle S_2 \rangle, \quad S_{\text{int}}^{(2)} = -\frac{\langle S_1^2 \rangle - \langle S_1 \rangle^2}{2}. \quad (11)$$

The integral of the term e^{-S_0} yields a W -independent factor to the partition function corresponding to the free energy F_0 calculated at the saddle point. The value of F_0 is given by (6), while N is the number of replicas. The symbol $\langle \dots \rangle$ denotes the average with respect to the ground state of the Hamiltonian (4). To calculate the terms $S^{(1)}$ and $S_0^{(2)}$, we use the identity $\langle \sin 2K \rangle = 0$, while the average value of $\cos 2K$ is determined by (7). The self-consistency equation provides $S^{(1)} = 0$ as it should be at the saddle point. The two remaining terms describe fluctuations near the saddle point. They can be written in the form

$$S_0^{(2)} = \sum_{a,b} \int \frac{d\varepsilon d\varepsilon'}{8\pi\delta} (\sqrt{\varepsilon^2 + \tilde{E}_g^2} + \sqrt{\varepsilon'^2 + \tilde{E}_g^2}) \times (c_{\varepsilon\varepsilon'}^{ab} c_{\varepsilon'\varepsilon}^{ba} + d_{\varepsilon\varepsilon'}^{ab} d_{\varepsilon'\varepsilon}^{ba}), \quad (12)$$

second term comes from small values $\varepsilon \lesssim \max\{\Omega, \tilde{E}_g\}$.

The analogous screening function for the correlator $D^{ab}(\varepsilon, \varepsilon'; \omega)$ is

$$\mathcal{D}(2\Omega) = \frac{\delta}{8} Y(2\Omega) \left[\log \frac{2\Delta}{\tilde{E}_g} - \frac{\operatorname{arcsinh}(\Omega/\tilde{E}_g)}{\sqrt{1 + \tilde{E}_g^2/\Omega^2}} \right]. \quad (26)$$

Now, everything is ready for the calculation of the derivative $\partial F/\partial(G^2)$. The preexponent in (19) contains the sum over a single replica index. The saddle point is trivial in the replica space. Therefore, this sum will be canceled by $1/N$. Another feature of the preexponent is the factor $2\pi\delta(0)$. This factor appears from the delta function in the definition of Cooperon (20). The same is also true for the diffuson term in the preexponent. At a finite temperature, $2\pi\delta(0) = 1/T$, which cancels the temperature in (19). Once this cancellation is established, we can safely assume that $T = 0$.

After the substitution of (24) and a similar expression for $D^{ab}(\varepsilon, \varepsilon'; \omega)$ into (19) and integration with respect to ω and the sum $\varepsilon + \varepsilon'$, we come to a single integral over $\Omega = \varepsilon - \varepsilon'$:

$$\frac{\partial F}{\partial(G^2)} = - \int \frac{d\Omega}{4\pi} \left[\frac{\mathcal{G}(\Omega)}{1 - G^2\mathcal{G}(\Omega)} + \frac{\mathcal{D}(\Omega)}{1 - G^2\mathcal{D}(\Omega)} \right]. \quad (27)$$

In the limit $G^2 = 0$, the vertex part of the action, $S_{\text{int}}^{(2)}$, is absent. This leads to the absence of the fluctuational contribution at $G^2 = 0$ in the limit $N \rightarrow 0$. Using this fact, we finally come to the full expression for the free energy by integrating (27)

$$F = F_0 + \int \frac{d\Omega}{4\pi} \log [1 - G^2\mathcal{G}(\Omega)][1 - G^2\mathcal{D}(\Omega)]. \quad (28)$$

The total Josephson current is now easy to find by differentiating the free energy $I = (2e/\hbar)\partial F/\partial\varphi$. The current derived from the first term F_0 was found in [1]. A rather simple expression (8) exists for this quantity. The fluctuational contribution is much more complicated. The dependence on the phase difference φ is contained not only in the factor G^2 according to (1) but also in the screening functions. The situation is very much simpler in the physically interesting limit of strong Coulomb blockade. The minigap is strongly suppressed, and the saddle point itself produces a negligible contribution to the Josephson current. In the fluctuational part of the free energy, we put $\tilde{E}_g = 0$. Expression (4) becomes a free particle Hamiltonian as $q = 0$. Only the first term is left in both sums (16) and (17); hence, $X(\omega) = Y(\omega) = 4E_C/(16E_C^2 + \omega^2)$. The screening functions (25) and

(26) become identical and contain only $\log(\Delta/\Omega)$ in square brackets. The dependence of the free energy on φ is now provided only by the factor G^2 in (28). For the Josephson current in the strong Coulomb blockade regime, we have

$$I(\varphi) = \frac{e\delta}{4\hbar} G_L G_R \sin\varphi \log \frac{\Delta}{2E_C}. \quad (29)$$

Thus, the result of [4] is reproduced.

In the opposite limit of the weak Coulomb blockade, the fluctuational contribution to the supercurrent is small in comparison with I_0 . When the phase difference changes from 0 to π , the system goes from a weak to strong Coulomb blockade regime. This means that the result (8) gradually transforms into (29). Numerical differentiating of (28) gives the solid curves plotted in the figure for the current-phase dependence. Note the local minimum that appears in the crossover region. There is no simple analytic theory for this effect. However, this is likely to be the most prominent feature of the system.

In conclusion, we have calculated the fluctuational correction to the free energy and to the Josephson current in the Coulomb blocked SINIS junction. This correction plays a major role in the limiting of strong Coulomb interaction. At intermediate values of the phase bias, a well-defined local minimum of the Josephson current appears.

We are grateful to I.S. Beloborodov and A.V. Lopatin for pointing out the fluctuational effect and for fruitful discussions of the calculations. This work was supported by the program ‘‘Quantum Macrophysics’’ of the RAS, by the Russian Ministry of Education and Science under contract no. RI-112/001/417, and by the Russian Foundation for Basic Research, project no. 04-02-16348-a. P.M.O. acknowledges the support of the Dynasty Foundation.

REFERENCES

1. P. M. Ostrovsky and M. V. Feigel'man, Pis'ma Zh. Éksp. Teor. Fiz. **79**, 602 (2004) [JETP Lett. **79**, 489 (2004)]; cond-mat/0404362.
2. P. M. Ostrovsky, M. A. Skvortsov, and M. V. Feigel'man, Phys. Rev. Lett. **92**, 176805 (2004); cond-mat/0311242.
3. I. S. Beloborodov and A. V. Lopatin, private communication.
4. C. Bruder, R. Fazio, and G. Schön, Physica B (Amsterdam) **203**, 240 (1994).
5. P. M. Ostrovsky, PhD Thesis (2004), <http://chair.itp.ac.ru/biblio/theses/2004/ostrov.pdf>.
6. A. A. Abrikosov, L. P. Gor'kov, and I. E. Dzyaloshinski, *Methods of Quantum Field Theory in Statistical Physics* (Fizmatgiz, Moscow, 1962; Dover, New York, 1963).

On the Privacy-Preserving Cascade Method for Correcting Errors in Primary Keys in Quantum Cryptography

A. V. Timofeev^a and S. N. Molotkov^{a, b}

^a Faculty of Computational Mathematics and Cybernetics, Moscow State University, Vorob'evy gory, Moscow, 119899 Russia

^b Institute of Solid State Physics, Russian Academy of Sciences, Chernogolovka, Moscow region, 142432 Russia

Received October 27, 2005

A general method is proposed for privacy protection upon correction of errors in primary keys in quantum cryptography through an open communication channel. By the example of the cascade procedure for correcting errors, a method is described for removing information sent through an open communication channel when cleaning a key. The critical percentage is found for the quantum cryptography protocol BB84 to which the cascade error correction method with deletion guarantees the security of the final key. The method proposed for removing information sent through the open communication channel is quite general and can be used for many cleaning protocols for primary keys in quantum cryptography. © 2005 Pleiades Publishing, Inc.

PACS numbers: 03.65.Bz, 03.67.Db

Quantum cryptography, which is a system of secure key distribution between remote users, makes it possible to transfer keys through an open quantum communication channel. Any quantum cryptography protocol of generating secure keys includes three stages [1, 2]. The first stage—the stage of generating primary keys—is the transmission of quantum states through the quantum communication channel and conduction of measurements at the receiver end by a certain protocol. The result of the measurements is a bit string, which generally differs from the bit sequence at the transmitter end. After the measurement results have been obtained, information is exchanged performed through an open classical communication channel, e.g., for agreement between the bases and estimation of the probability of errors at the receiver end as in the most widespread protocol BB84 [1]. In this case, a part of the bit sequence is opened and then open positions are removed. As a result of the first stage of the protocol, a primary key arises for legitimate users (usually named Alice and Bob).

Any quantum cryptography system guarantees the security of keys if the percentage of errors at the receiver end does not exceed a certain critical value [3–5]. Otherwise, the protocol is interrupted.

At the end of the first stage, an eavesdropper (usually named Eve) already *can have*¹ certain information on the primary key, which he can acquire from the quantum communication channel during the transmission of quantum states. Further information exchanges

between the legitimate users through the open classical communication channel cannot increase the eavesdropper's information on the primary key, because the open positions are omitted.

The second stage of the protocol is the correction of errors by means of exchange of classical information through the open classical communication channel. The correction of errors at the receiver end is in essence a classical procedure. The fundamental difference of this procedure from conventional error-correction methods in classical information theory is that it is performed between remote users and all auxiliary information transmitted through the open communication channel is assumed to be known to the eavesdropper. The main requirement imposed on the error correction procedure is protection of privacy. In other words, the correction of errors should not increase the information known to the eavesdropper about the “clean” key that he has acquired up to this stage. In this case, Alice and Bob are forced to omit some bits in the primary sequence. According to the second requirement referring to the procedure efficiency, the clean key must be as long as possible.

Strictly speaking, the critical error to which the protocol ensures the security of keys, the efficiency of the error correction procedure in the primary keys, and the length of the final key are closely related to each other. For example, the maximum allowable critical error (11%) for the protocol BB84 is achieved when errors are corrected by means of random codes (the Shannon limit [6]), which are not constructively realizable, because they require an exponentially large set of code words over the length of the bit sequence. The maximum of the minimum code distance is reached on random code words. In this case, if the sequence is suffi-

¹ In this context, “can” means the following. Generally speaking, the eavesdropper can acquire information on the final key at the last stage by, e.g., storing his quantum states in quantum memory when all the auxiliary exchanges by classical information between the legitimate users are completed.

ciently long (formally for $n \rightarrow \infty$) and the error probability is less than the critical value, the entire length of the bit sequence after the correction of errors can be taken as the final secure key. If errors are corrected with codes on which the Varshamov–Hilbert rate boundary [7] is reached, the admissible error percentage does not exceed 7.5% [3–5]. In this case, after the correction of errors, the entire sequence also can be taken as the final secure code.

The use of constructive codes when correcting errors is the forward correction of errors; i.e., in dependence of the observed error percentage, a set of code words that are openly announced is chosen. Errors at the receiver end are corrected by means of a calculated syndrome. In this case, the critical error percentage to which the protocol guarantees the security of the *entire* corrected bit sequence depends on the redundancy of the code. In this approach, the critical error should be calculated separately for each code.

More practically convenient are iteration error correction procedures, which are reduced to the calculation of parities of various subsets of the primary key and bilateral exchange of information on these parities through the open communication channel. In this case, the parities of these subsets become known to the eavesdropper. If some bits are removed in a certain way, either in the cleaning process or after its completion, the eavesdropper cannot acquire additional information compared to the information that he had before the error correction procedure.

The third stage of the protocol is the privacy amplification or the compression of the clean key [8]. After the correction of errors and the deletion of some bits, a shorter bit sequence remains for legitimate users. The eavesdropper's information about this string is limited by the initial information that he could acquire from the quantum communication channel. Thus, if it were possible to find a reliable upper bound for the information that the eavesdropper can acquire from the quantum communication channel, the problem of the extraction of the secure key from the primary bit sequence would be constructively solved. This information can be reduced to an exponentially small value in a chosen security parameter by compression (hashing of the clean key by means of universal homogeneous functions of the second kind [8, 9]).

Cascade method of error correction (CASCADE).

The simplest iteration procedure of error correction is the bisection search for error, which is reduced to the division of the primary key into random nonoverlapping blocks and to the calculation of the parities of these blocks. The parities of sets at the receiver and transmitter ends are compared through the open channel. After the parity of a certain set is opened, one of the randomly chosen bits is removed. If the parities do not coincide, the size of the block is halved and the process is repeated. Since the blocks do not overlap, the deletion of bits is simple. Such a procedure protects the pri-

vacuity; i.e., the eavesdropper does not acquire additional information upon the cleaning of the primary key. However, such a procedure is extremely inefficient, because a few bits remain in the clean key (e.g., for an error probability of 10% in the primary key, no more than 10% of the initial length remains in the clean key).

In terms of the length of the clean key, the cascade error correction method proposed in [10] is most efficient at present. In the initial variant of the cascade method, the parity bits of the individual and generally *overlapping* subsets are stored and used in the next passes. In this method, no bits are deleted. For this reason, the method does not protect privacy. It is difficult to estimate the information that is acquired by the eavesdropper when opening the parity bits of overlapping subsets that appear in different passes. As far as we know, a complete analysis has not yet been performed.

The privacy and efficiency of the method can be retained if a certain number of bits are deleted at the end of the cleaning of the primary key. Since the bit sets arising in each pass overlap with each other, such a deletion procedure is not trivial.

In this work, a simple regular method for retaining privacy is proposed. For convenience, we first describe the cascade method of error correction without deletion.

The CASCADE algorithm consists of several passes over the primary key. At each pass, the key is randomly divided into blocks of a certain size by means of auxiliary hash functions and the errors in these blocks are sought according to the algorithm described below. The number of passes and the size of the blocks are determined in advance from the error probability in the primary key by the method described in [10].

Each pass consists of the following steps.

(i) The key is divided into blocks by means of auxiliary hash functions: the m th block includes bits with numbers satisfying the condition $f_k(i) = m$. The function is taken in the class of universal hash functions [9].

(ii) Alice and Bob calculate the parities of their blocks and compare them. If the parities of a certain block do not coincide for Alice and Bob, this block contains an odd number of erroneous bits. In this block, the error can be found by bisection search: Alice and Bob bisect this block and compare the parities of the first half of the block. If they coincide, the second half contains an odd number of errors; otherwise, an odd number of errors are in the first half. The block half containing errors is again bisected and the process continues until the error is localized. Then, Bob corrects the erroneous bit.

(iii) In passes beginning with the second pass, the error found can be used for finding other errors. Let i and k be the erroneous bit number and pass number, respectively. The i th bit belonged to certain blocks at the preceding passes. The parity of each of such block changes and the errors in these blocks can be found



Fig. 1.

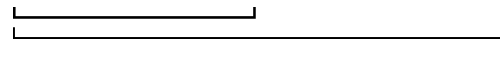


Fig. 2.



Fig. 3.

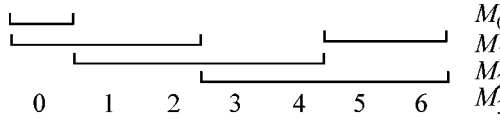


Fig. 4.

using the same method. We construct the set \mathcal{H} from these blocks, take one block from this set, and find one more error in it. Let j and \mathcal{M} be the erroneous bit number and the set of blocks containing this bit, respectively. Then, all the blocks containing the j th or i th bit but not both bits together contain an odd number of errors. We find an error in a new set $\mathcal{H}^* = \mathcal{M} \nabla \mathcal{H}$ that is equal to the symmetric difference between the sets \mathcal{H} and \mathcal{M} . This process continues until that the new set \mathcal{H} becomes empty.

Experience shows that four passes over the key is enough to clean all the errors in the overwhelming majority of cases. In order to verify that all the errors are corrected, we compose N random subsets of key bits and compare their parities. The probability that a key with errors passes such verification is equal to 2^{-N} .

Information known to the eavesdropper. Let us analyze what information on the key is acquired by the eavesdropper due to the operation of the cascade. As usual in quantum cryptography, we suppose that the eavesdropper knows hash functions and all the parameters of the protocol operation. In this case, he acquires the parity bits for blocks at each pass and receives $\log(\text{block size})$ parity bits of block subsets per found error. The blocks in one pass do not overlap and each subset obtained due to the search for an error is completely embedded either in a certain other subset or in the block as a whole (Fig. 1). As a result of the verification of the key, additional N parity bits are opened. Thus, all the information known to the eavesdropper is a certain number of parity bits of the key subsets.

Privacy protection. If there is only one set for which the parity bit is known, this information can be deleted by deleting any bit from this set (provided that the bit values 0 and 1 are equiprobable), because different bit values correspond to different parities. Let us consider two sets, one of which is embedded in the other (see Fig. 2). The knowledge of the parity bits of these sets is evidently equivalent to the knowledge of the parities of these sets (Fig. 3). Then, we consider a system of overlapping sets M (Fig. 4). It is necessary to find a bit set B such that, after its deletion, all information on the parity of these sets disappears. This means

that all possible values of the parities of M can be obtained by searching through the bit values of B . Such a set exists (e.g., all the bits). Let us determine the least such set. A change in one bit leads to a change in the parity of all the sets containing this bit. For each bit B_i , we compose the bit vector V_i in which the bit V_i^j is equal to unity if $B_i \in M_j$:

$$\begin{aligned} V_1 &= (1, 1, 0, 0), \\ V_2 &= (0, 1, 1, 0), \\ V_3 &= (0, 1, 1, 0), \\ V_4 &= (0, 0, 1, 1), \\ V_5 &= (0, 0, 1, 1), \\ V_6 &= (0, 1, 0, 1), \\ V_7 &= (0, 1, 0, 1). \end{aligned}$$

A change in the bits i_1, \dots, i_k results in a change in the parity of all the sets containing unity in the linear combination $V_{i_1} + \dots + V_{i_k}$. Therefore, if one of the vectors V_i is a linear combination of other vectors, new parity values cannot be obtained by means of the i th bit. Thus, the bits whose vectors form the base of the vectors V can be taken as the set B .

The base can be found by reducing the matrix composed from these vectors to the step form by the Gauss method. First, we change the system of sets (M) in order to reduce the number of unities in the matrix. Omitting all repeated vectors, we obtain

$$\begin{aligned} V_1 &= (1, 1, 0, 0), \\ V_2 &= (0, 1, 1, 0), \\ V_4 &= (0, 0, 1, 1), \\ V_6 &= (0, 1, 0, 1). \end{aligned}$$

Each system of sets obtained as a result of the search for one error can be represented as a system of nonoverlapping sets (Fig. 5). After this operation, no sets obtained in one pass of the cascade overlap with each other, and, therefore, each row of the matrix contains no more than

four bits (except for N testing bits). For the example under consideration, we obtain the system shown in Fig. 6. Correspondingly, the vectors have the form

$$\begin{aligned} V_1 &= (1, 0, 0, 0), \\ V_2 &= (0, 1, 1, 0), \\ V_4 &= (0, 0, 1, 1), \\ V_6 &= (0, 1, 0, 1). \end{aligned}$$

We place the sets in order of increasing power:

$$|M_1| < |M_2| < \dots < |M_m|,$$

$$\begin{aligned} V_1 &= (1, 1, 0, 0), \\ V_2 &= (0, 1, 1, 0), \\ V_4 &= (0, 0, 1, 1), \\ V_6 &= (0, 1, 0, 1). \end{aligned}$$

The matrix can now be stored in the sparse form and the Gauss method requires many fewer operations. The Gauss method yields the matrix

$$\begin{aligned} V_1 &= (1, 1, 0, 0), \\ V_2 &= (0, 1, 1, 0), \\ V_4 &= (0, 0, 1, 1), \\ V_6 &= (0, 0, 0, 0). \end{aligned}$$

Therefore, it is sufficient to delete three bits with the numbers 1, 2, and 4.

Compression degree of the clean key. The compression degree of the clean key depends on the efficiency of the error correction procedure or, more precisely, on the redundancy. The use of random code words (Shannon limit) makes it possible to obtain the maximum number of information bits $nH(Q)$, where n is the sequence length, $H(Q) = 1 + Q\log(Q) + (1 - Q)\log(1 - Q)$, and Q is the error probability. Correspondingly, the redundancy of a random code is equal to $n(1 - H(Q))$. The Shannon random code has the maximum minimum distance (minimum redundancy) as compared to other codes. Other procedures of error correction provide large redundancy. In other words, the *information opened in bits* when correcting errors cannot be less than $n(1 - H(Q))$. The larger the redundancy of the error correcting code, the shorter the final key and the smaller the critical error to which the security of the key is guaranteed. Figure 7 shows the redundancy for the Shannon random code and for the CASCADE procedure with deletion.

Let us use the consequence of the fundamental privacy-amplification theorem [8]. Eve's strategy is described by an arbitrary function $E: \{0, 1\}^{n_{AB}} \rightarrow \{0, 1\}^t$; i.e., Eve knows no more than t bits for an arbitrary string of n_{AB} bits, where n_{AB} is the bit string for Alice and Bob after error correction. Let s be the security

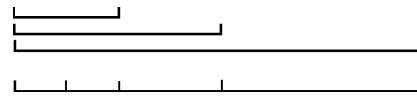


Fig. 5.

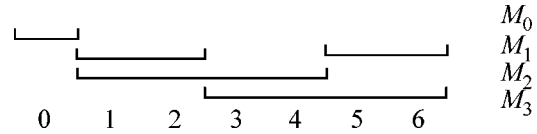


Fig. 6.

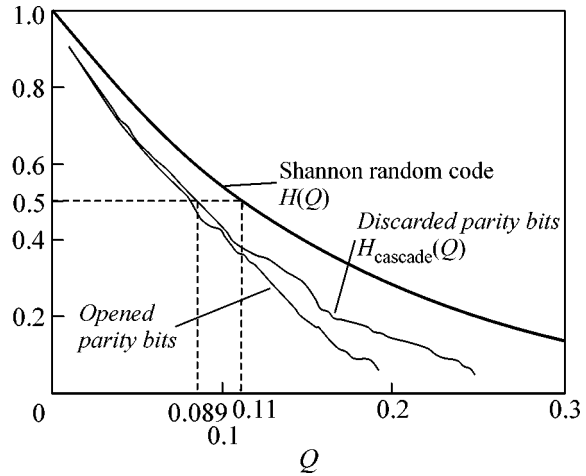


Fig. 7. Error correction by the CASCADE procedure with deletion was performed for a sequence with a length of 10^4 bits.

parameter ($s < n_{AB} - t$), and $G: \{0, 1\}^n \rightarrow \{0, 1\}^r$ is a universal homogenous hash function of the second kind [9, 8], which itself is random. Then, the mutual information $K = G(X)$ known to Eve on the secure key does not exceed

$$I(K; GZ) \leq 2^{-s} / \ln 2. \tag{1}$$

Let $Z: \{0, 1\}^t$ be Eve's string consistent with the string X of the legitimate users; i.e., this string can follow from strings X as $Z = E(X)$. We aim to calculate the length r of the final key about which Eve has information exponentially small in s . To this end, it is necessary to know the second-kind Renyi entropy, which, in turn, is expressed in terms of the collision probability.

For quantum cryptography (BB84 protocol), Eve can distinguish no more than $2^{\frac{n\bar{C}(\rho)}{2}}$ strings, where $\bar{C}(\rho)$ is the classical capacity of the quantum communication channel [11], among the general set $2^{nH_{\text{CASCADE}}(Q)}$, which is the number of possible strings that Alice and Bob know after the error correction by

the CASCADE procedure. In other words, $n_{AB} = nH_{\text{CASCADE}}(Q)$ is the length of the bit string that remains after the error correction by the CASCADE procedure with deletion (n is the string length before the error correction).

The conditional probability is determined by the ratio of the total number of strings to the number of decoding regions used by Eve:

$$P_{X|Z=z} = \frac{2^{\frac{n\bar{C}(\rho)}{2}}}{2^{nH_{\text{CASCADE}}(Q)}} = 2^{-n\left(H_{\text{CASCADE}}(Q) - \frac{\bar{C}(\rho)}{2}\right)} = a_z. \quad (2)$$

In fact, $1/a_z$ is the fraction of strings such that $z = E(X)$; i.e., each partial string of Eve's is consistent with the set of strings determined by Eq. (1). The collision probability is given by the expression

$$\begin{aligned} P_c(X|Z=z) &= \sum_{X: \{z=E(X)\}} P_{X|Z=z}^2 \\ &= 2^{-n\left(H_{\text{CASCADE}}(Q) - \frac{\bar{C}(\rho)}{2}\right)} = \frac{1}{a_z^2}. \end{aligned} \quad (3)$$

The second-kind Renyi entropy is equal to

$$\begin{aligned} R(X|Z=z) &= -\log P_c(X|Z=z) \\ &= n\left(H_{\text{CASCADE}}(Q) - \frac{\bar{C}(\rho)}{2}\right). \end{aligned} \quad (4)$$

According to the theorem of privacy amplification [8],

$$H(K|G, Z=z) \geq r - 2^{r-R(X|Z=z)}/\ln 2 > r - 2^r/a_z \ln 2. \quad (5)$$

Taking into account that $P_Z(z) = 1/2^{n\bar{C}(\rho)/2} = 2^{-nH_{\text{CASCADE}}(Q)}/a_z$, we obtain the mutual information between Eve's strings and the secure key of Alice and Bob in the form

$$\begin{aligned} I(K; GZ) &= H(K) - H(K|GZ) \\ &\leq r - \sum_{z \in \{0,1\}^t} P_Z(z) H(K|G, Z=z) \\ &\leq \sum_{z \in \{0,1\}^t} a_z 2^{-nH_{\text{CASCADE}}(Q)} \frac{2^r}{a_z \ln 2} \\ &= 2^{-nH_{\text{CASCADE}}(Q) + t + r} / \ln 2 = 2^{-s} / \ln 2. \end{aligned} \quad (6)$$

The length of the secure key $K = G(X) \in \{0, 1\}^r$ is given by the formula

$$r = n\left(H_{\text{CASCADE}}(Q) - \frac{\bar{C}(\rho)}{2}\right) - s. \quad (7)$$

For the BB84 protocol, $\bar{C}(\rho) = 1$. Correspondingly, the cleaning of the primary key by the CASCADE procedure with deletion ensures the security of the final key if the error percentage does not exceed $Q_{\text{CASCADE}} \approx 8.9\%$ [Q_{CASCADE} is determined as the root of the equation $H_{\text{CASCADE}}(Q_{\text{CASCADE}}) = \bar{C}(\rho)/2$]. When errors are corrected by random code words (Shannon limit), the BB84 protocol is secure to $Q_c \approx 11\%$ ($H(Q_c) = \bar{C}(\rho)/2$).

The privacy protection method described above is quite general and can be used for other error correction procedures.

This work was supported by the Russian Foundation for Basic Research (project nos. 05-02-17387a and 02-208306of) and the Russian Federal Agency for Science and Innovation (contract no. 02.435.11.1004). S.N.M. acknowledges the support of the Academy of Cryptography of the Russian Federation.

REFERENCES

1. C. H. Bennett and G. Brassard, in *Proceedings of IEEE International Conference on Computer Systems and Signal Processing, Bangalore, India, 1984* (IEEE, New York, 1984), p. 175.
2. C. H. Bennett, F. Bessette, G. Brassard, *et al.*, *J. Cryptology* **5**, 3 (1992).
3. D. Mayers, quant-ph/9802025.
4. E. Biham, M. Boyer, P. O. Boykin, *et al.*, quant-ph/9912053.
5. P. W. Shor and J. Preskill, quant-ph/0003004.
6. C. E. Shannon, *Bell Syst. Tech. J.* **27**, 397 (1948); *Bell Syst. Tech. J.* **27**, 623 (1948).
7. E. J. Mac Williams and N. J. A. Sloane, *The Theory of Error-Correcting Codes* (North-Holland, Amsterdam, 1977).
8. C. H. Bennett, G. Brassard, C. Crépeau, and U. Maurer, *IEEE Trans. Inf. Theory* **41**, 1915 (1995).
9. J. L. Carter and M. N. Wegman, *J. Comput. Syst. Sci.* **18**, 143 (1979).
10. G. Brassard and L. Salvail, in *Advances in Cryptology, Eurocrypt'93*, Ed. by T. Hellesteth (Springer, Berlin, 1994), p. 410; *Lect. Notes Comput. Sci.* **765**, 410 (1994).
11. A. S. Kholevo, *Probl. Peredachi Inf.* **8**, 63 (1972); *Probl. Peredachi Inf.* **15**, 3 (1979); *Usp. Mat. Nauk* **53**, 193 (1998); *Introduction to Quantum Information Theory* (MTsNMO, Moscow, 2002), *Sovrem. Mat. Fiz.*, No. 5.

Translated by R. Tyapaev

In Memory of Our Authors

V. M. Aul'chenko, ..., J. A. Thompson, ..., V. W. Hughes, et al., *Measurement of the Pion Form Factor in the Range 1.04–1.38 GeV with the CMD-2 Detector*, *Pis'ma Zh. Éksp. Teor. Fiz.* **82, 841 (2005)** [*JETP Lett.* **82, 743 (2005)**].

Professor Julia Ann Thompson, age 61, was killed in a car accident on August 16, 2004. After graduation from Yale University, she worked at the Faculty of Physics and Astronomy, Pittsburg University, in experimental particle physics. Ms. Thompson participated in experimental programs at the world's largest accelerator centers: CERN, Switzerland; Brookhaven National Laboratory, United States; and the Budker Institute of Nuclear Physics, Russia. She was involved in international collaborations, made a significant contribution to solving many important problems in particle physics, and published more than 100 scientific papers.

V. M. Aul'chenko, ..., J. A. Thompson, ..., V. W. Hughes, et al., *Measurement of the Pion Form Factor in the Range 1.04–1.38 GeV with the CMD-2 Detector*, *Pis'ma Zh. Éksp. Teor. Fiz.* **82, 841 (2005)** [*JETP Lett.* **82, 743 (2005)**].

Professor Vernon W. Hughes, age 81, passed away on March 25, 2003. In 1950, he received his PhD at Columbia University, New York, where he, together with colleagues, observed two-photon transitions in atomic spectroscopy for the first time. His scientific interests covered a wide range from the lowest to the highest energies. For 30 years, he studied helium atoms

and positronium and observed muonium for the first time in 1960. These experiments opened a new direction in experimental investigations of quantum electrodynamics and the search for new phenomena beyond the framework of the Standard Model.

Hughes was one of the pioneers of another very important direction—the use of polarized electrons in high- and low-energy accelerators. Studying the deep inelastic scattering of polarized muons on polarized protons and neutrons, the collaboration led by Hughes at CERN discovered a new phenomenon called “proton spin crisis.” Investigation of this phenomenon is far from completion, but it has already led to a serious reevaluation of the relation between the internal structure of the proton and its spin. To date, Hughes was the inspiration and scientific leader of a brilliant experiment on measuring the anomalous magnetic moment of the muon at Brookhaven National Laboratory. This parameter is determined by all existing interactions, and its comparison with calculation provides verification of new ideas in particle physics.

Hughes always focused his interests on the most fundamental problems in physics. Precise experimental procedures developed by him made it possible to measure a number of fundamental constants determining the mysterious properties of our universe.

Translated by R. Tyapaev

In Memory of Igor' Il'ich Sobel'man

Member of the Editorial Board of *JETP Letters* from 1969 to 1988

Igor' Il'ich Sobel'man, outstanding scientist, Director of the Optics Division at the Lebedev Physical Institute of the Russian Academy of Sciences (RAS), Corresponding Member of the RAS, and professor at the Moscow Institute of Physics and Technology, passed away suddenly on November 23, 2005. For many years, he was a member of the Editorial Board of *JETP Letters*. It was this Editorial Board that determined the style of the journal for many years to come.

Sobel'man was born on January 26, 1927, in Moscow and graduated from the Faculty of Physics and Engineering of Moscow State University in 1952 (among the first graduating body from this faculty). All his scientific and pedagogical activity was connected with the Lebedev Physical Institute of the RAS and the Moscow Institute of Physics and Technology, where he manifested his brilliant talent as a scientist and a teacher. Sobel'man had wide scientific interests and intuition in the field of physics; it was his goal to solve great physical problems and he had the rare ability to clearly formulate the essence of such problems. One of Sobel'man's characteristic features was his ability to successfully develop theoretical methods and approaches from various areas of physics and apply them to urgent problems in optics, spectroscopy, and quantum radiophysics, in combination with experimental possibilities.

Sobel'man was among the authors who created the current theory of the broadening of spectral lines. He made a considerable contribution to the physics of atomic collisions, and he formulated and solved a number of problems in nonlinear laser spectroscopy and laser frequency standards. Sobel'man proposed new methods for creating high-powered lasers, including photodissociation lasers, far-UV and soft x-ray lasers,

and fundamentally new stimulated-scattering-based light-beam converters. Under his supervision, measurements of parity violation in atomic physics were conducted, a method of polarizing the nuclear spin of ^3He in a dense gas was realized, and a number of unique studies concerning solar x-ray astronomy were performed. In recent years, Sobel'man worked enthusiastically on the problem of time-reversal violation in atomic physics. He proposed a new method of determining the electric dipole moment that arises in the xenon atom due to this effect. Sobel'man made a great contribution to the education of scientists in optics, spectroscopy, and quantum radiophysics in the USSR and Russia. When he was a young scientist, he wrote a unique monograph that even today is used as a reference book on atomic spectroscopy. For many years, he gave lectures on physical optics and spectroscopy at the Moscow Institute of Physics and Technology. His scientific and pedagogical activity significantly affected the formation of several generations of scientists in optics and spectroscopy. He was a member of the editorial boards of several domestic (including *JETP Letters*) and foreign publications, and he was the chairman of the scientific council "Atomic and Molecular Spectroscopy" of the RAS.

Igor' Il'ich Sobel'man was not only a brilliant scientist but also a remarkable person. He made wise and balanced decisions, his interests and erudition were wide, and he possessed a fine sense of humor. His passing is an irreplaceable loss to all his friends and colleagues.

Translated by R. Tyapaev